THE ASTROPHYSICAL JOURNAL, 246:761–787, 1981 June 15

MOLECULAR CLOUDS ASSOCIATED WITH COMPACT H II REGIONS. I. GENERAL PROPERTIES

PAUL T. P. HO[1]
Radio Astronomy Laboratory, University of California, Berkeley; and
Department of Physics and Astronomy, University of Massachusetts, Amherst
ROBERT N. MARTIN
Max Planck Institute for Radioastronomy
AND
ALAN H. BARRETT
Department of Physics, Massachusetts Institute of Technology
Received 1980 July 24; accepted 1980 December 30

ABSTRACT

Very compact H II regions with typical sizes less than 0.1 pc, excited by stars with spectral types B2 to O7, are found associated with warm and dense molecular clouds. Typical values of $n(H_2) > 10^4$ cm^{-3}, $T_k = 20$–40 K, and $M = 10^2$–10^4 $M_\odot$ are deduced from molecular line studies of NH_3, CS, and CO. These regions are suggested to be the less evolved versions of a molecular cloud–H II region complex such as in Orion. A clumpy structure in the NH_3 emission cannot be ruled out. If this is important, $n(H_2) > 10^5$ cm^{-3}, and the presence of small hot cores with size scales ~ 0.1 pc $(T_{ex}/50$ K$)^{-1/2}$ is implied. The deduced masses, the fraction of the total H_2 column density residing within the condensations, and the ability of dust to heat the gas are all influenced by the presence of clumpy structures within the molecular clouds. A rough correlation is found between the maximum stellar mass in a region and the mass of the associated molecular cloud condensation. The association of stars of spectral types later than B0 with cloud mass less than 10^2 $M_\odot$ appears to imply that the cloud was already fairly dense [$n(H_2) > 10^3$ cm^{-3}] prior to the collapse and fragmentation process as described by Larson.

Subject headings: interstellar: molecules — nebulae: general — stars: formation

I. INTRODUCTION

According to current star formation theories, the final infall and accretion of matter onto the stellar core will be halted by gas and radiation pressures as nuclear burning begins. An ionization front will expand from the stellar surface, forming an H II region. With sufficient sensitivity, the radiation from electron-proton bremsstrahlung in this ionized region can be detected in the continuum at microwave frequencies. Hence this early stage of stellar evolution, with the placental cloud essentially intact and while the star is still optically obscured by dust (Davidson and Harwit 1967), can be studied handily via radio astronomy techniques. It has been known for some time that small scale structures (<0.5 pc) with high densities ($>10^4$ cm^{-3}) exist in H II regions (Ryle and Downes 1967; Mezger, Schraml, and Terzian 1967). But it was the development of synthesis radio telescopes achieving angular resolution on the order of arc seconds, that led to the discovery of very compact radio structures. From a study of a group of H II regions in the Perseus arm, Israel, Habing, and de Jong (1973) distinguished between compact H II regions (CHII) and ultracompact H II regions (UCHII). The CHII regions are defined to have diameters 0.1 pc$< d <$1 pc with a range of electron densities 10^4 cm$^{-3} > n_e > 10^3$ cm^{-3} while the UCHII regions are defined to have $d < 0.1$ pc and $n_e > 10^4$ cm^{-3}. It is this latter group of H II regions to which we will principally be addressing ourselves in this paper. The readers are referred to Habing and Israel (1979) for a review of both CHII and UCHII regions.

Habing *et al.* (1974) have suggested that the UCHII region is the first stage of an evolutionary sequence for a massive star which eventually develops through the CHII stage into a full-grown H II region. Whereas the CHII stage is believed to be density bound, the UCHII stage is probably ionization bound as dense shells of neutral matter appear to surround these objects. In fact, some of the UCHII regions have been suggested to be the long sought cocoon stars (Kahn 1974). In any event, whether they are density bound or ionization bound, it is commonly believed that both the CHII and UCHII regions will expand rapidly (Vandervoort 1963*b*; Mathews 1965). This is due to the fact that

[1]Miller Fellow 1979–1981.

the pressure $P \propto nT \gtrsim 10^7$ cm^{-3} K within the ionized region, which is at least three orders of magnitude greater than the ambient values even for the ionization bound case. In addition, magnetic forces may not be negligible, as was suggested by Vandervoort (1963*a*). VLBI measurements of OH maser sources associated with UCHII regions such as W3(OH) indicate that magnetic fields on the order of a few milligauss are needed to explain opposite circularly polarized components of the maser emission (Moran *et al.* 1978; Lo *et al.* 1975; Harvey *et al.* 1974). If the same magnetic field permeates the region around the OH masers, an equivalent pressure of $nT \sim 10^{10}$ cm^{-3} K due to the magnetic forces must also be dealt with in the expansion of the H II regions. Thus a direct estimate of the dynamical age for these regions can be difficult. Nevertheless one may infer from their close association with OH masers (Habing *et al.* 1974), and the more distant association with H_2O masers (Lo, Burke, and Haschick 1975; Forster, Welch, and Wright 1978), that the CHII and UCHII regions are probably young objects with ages less than 10^5 years (cf. Habing and Israel 1979).

Whatever their ages are, the compact spatial structures of the UCHII regions suggest that insufficient time has elapsed for the ambient cloud matter to be disrupted or dispersed. These regions therefore provide an opportunity to study the properties of a star-forming region after stellar densities are reached. We conducted a study of a sample of UCHII regions in the $(J, K)=(1,1)$ and $(2,2)$ inversion lines of NH_3. Supplementary studies were also conducted in the $J=1-0$ and $J=2-1$ rotational lines of CS, as well as the $J=1-0$ rotational line of CO and ^{13}CO. The objective was to assess the physical conditions of the neutral material surrounding these regions. Specifically we sought to improve our understanding of these regions by answering the following questions: (1) If there is neutral matter surrounding the UCHII regions, what are the densities and what are the temperatures? (2) As the UCHII regions are connected with the very last stages of star formation, are they located at local maxima in the NH_3 emission corresponding to temperature and/or density peaks? (3) If detected, what are the sizes and masses of the emission regions? Are these regions stable against collapse? (4) What is the role of the UCHII regions on the ambient cloud environment?

Although the measurement of hyperfine structures of the NH_3 inversion lines allows one to determine the excitation temperature and hence the local density, the possible problem of small scale structures (<0.1 pc) in NH_3 emission (Barrett, Ho, and Myers 1977; Schwartz *et al.* 1977) complicates the analysis. NH_3 observations were therefore conducted with different antenna beamwidths in order to assess the beam dilution problem. The CS studies of two of the regions were intended to provide an independent estimate of the density. Similarly, measurements of the optically thick CO emission provide an independent handle on the kinetic temperature, which will be able to compare with the rotational temperature deduced from our measurements of the (1,1) and (2,2) lines of NH_3.

We present our observations and analysis of the data in § II, our discussion on the nature of the molecular clouds which we have found in § III, and a summary of our conclusions in § IV. A later paper will discuss the individual clouds in more detail.

II. OBSERVATIONS AND DATA ANALYSIS

a) *Equipment*

Because the observing techniques differ substantially for the three molecules which we studied, we will describe the observing procedures in some detail.

i) NH_3

The NH_3 observations were obtained using the 36.6 m radio telescope of the Haystack Observatory[2] in Westford, Massachusetts, and the 100 m radio telescope of the Max-Planck-Institut für Radioastronomie in Effelsberg, West Germany. At Haystack, the receiver system consisted of a traveling wave maser preamplifier followed by a crystal mixer. The single-sideband system temperatures were typically 100–150 K. The spectrometer was a 100-channel autocorrelator, although a 1024-channel autocorrelator was also used in parallel on occasions to achieve higher spectral resolution. A total bandwidth of 6.67 MHz was sampled with effective resolutions of 166.7 kHz (2.1 km s^{-1}) and 16.3 kHz (0.21 km s^{-1}) for the two correlators. Except for S140, no serious filter dilution effects were found using the coarser resolution. At $\lambda \sim 1.3$ cm, we estimate the beamwidth of the antenna to be $\sim 1'.4$, and the beam efficiency to be ~ 0.25. At Effelsberg, the receiver was a cooled parametric amplifier whose single-sideband system temperature was ~ 180 K at zenith. The spectrometer was a 384-channel autocorrelator operating in the parallel mode with one half of the channels centered at the $(J, K)=(1,1)$ line and the other half centered at the (2,2) line. A total bandwidth of 5 MHz was sampled by each half of the autocorrelator yielding a spectral resolution of 63 kHz (0.80 km s^{-1}). At $\lambda \sim 1.3$ cm, only the inner 80 m of the antenna was illuminated. We estimate the beamwidth to be $\sim 43''$ and the beam

[2]Radio astronomy at the Haystack Observatory of the Northeast Radio Observatory Corporation is supported by the National Science Foundation under grant AST78-18227.

efficiency to be ~ 0.40 at zenith. The observing technique at both telescopes was position switching at the rate of once every 10 minutes. Noise tube calibrations were used to measure the system temperatures. Both the elevation-dependent gain variations of the antennas and the atmospheric attenuation have been corrected for in our data. We have also divided the antenna temperatures by their respective beam efficiencies, thus arriving at ΔT_a^*, the beam diluted brightness temperatures.

ii) CS

The CS observations were obtained using the 11 m millimeter wave antenna of the National Radio Astronomy Observatory[3] at Kitt Peak, Arizona. Both receivers at the $J=1-0$ ($\lambda \sim 6$ mm) and $J=2-1$ ($\lambda \sim 3$ mm) frequencies consisted of cooled mixers which accepted dual polarizations. However, because of the unequal noise characteristics of the mixers, one polarization being always significantly better, we in general observed only one polarization. Spectral analysis at Kitt Peak was accomplished by the use of two filter banks: 256×100 kHz and 128×30 kHz, operating in parallel. The velocity resolutions were therefore 0.61 and 0.18 km s^{-1} at $\lambda \sim 6$ mm, and 0.31 and 0.092 km s^{-1} at $\lambda \sim 3$ mm. At $\lambda \sim 6$ mm, we measured the double-sideband receiver temperature to be 478 K. Spectral line calibrations on DR 21 (OH) were performed with and without a waveguide image rejection filter with zero transmission at image frequency (Ulich 1979). This allowed us to estimate the signal sideband gain of the receiver to be $G_s \sim 0.90$. Hence the particular tuning configuration of the receiver during our experiment at 6 mm resulted in essentially a single-sideband system. As the transmittance of the waveguide filter at signal frequency was determined to be only 0.80 ± 0.03 from hot-cold load measurements and the spectral line calibrations, the $J=1-0$ CS observations were conducted in the double sideband mode. Zenith opacity of the atmosphere and the antenna efficiency coupled to the sky, which does not account for spillover η_{sp} (Ulich and Haas 1976), were determined from antenna tipping measurements to be $\tau_z = 0.22 \pm 0.02$ and $\eta_{sky} = 0.84 \pm 0.02$. The antenna beam width was determined from continuum scans on Saturn to be $\sim 2'.7$. Continuum measurements also served to check the antenna pointing and focusing of the subreflector. At $\lambda \sim 3$ mm, we measured the double-sideband receiver temperature to be 288 K. Spectral line calibrations on DR 21 (OH) together with hot-cold load measurements were made with and without an image rejection Fabry-Perot mesh filter. The signal sideband gain G_s and the transmittances of the filter t_s and t_i at signal and image frequencies were solved for simultaneously assuming $t_s + t_i = 1$. We found $G_s \sim 0.65$, $t_i \sim 0.1$, and $t_s \sim 0.9$. Because of the loss in the filter, observations of the $J=2-1$ line of CS were also made in the double-sideband mode. Values of τ_z and η_{sky} were once again estimated from antenna tipping to be 0.07 ± 0.02 and 0.73 ± 0.02, respectively. The usual continuum measurements were made on Saturn obtaining a beamwidth at $\lambda \sim 3$ mm of $\sim 1'.5$.

Finally in order to arrive at a value for the beam efficiency $\eta_b = \eta_{sky}\eta_{sp}$, η_{sp} was assumed to be 0.8. We therefore estimate $\eta_b \sim 0.67$ and 0.58 at $\lambda \sim 6$ mm and 3 mm, respectively. With these values for G_s, η_b, and τ_z, we then observed at both frequencies in the total power mode, position switching at the rate of once per minute. Values for ΔT_a^* were then obtained via the chopper wheel technique with the appropriate values for T_c.

We note that calibrations at millimeter wavelengths are indeed uncertain at best. Our estimates of η_{sky} and τ_z are based on the assumptions $T_s \approx T_i = T_m \sim 280$ K and $T_{sbr} \sim 280$ K, where T_s and T_i are the atmospheric temperatures at signal and image frequencies with T_m being the mean temperature, and T_{sbr} is the ground pickup temperature (see Ulich and Haas 1976). Perhaps the least certain of these assumptions is the value of T_{sbr}. We estimate that a change in the value of T_{sbr} by 40 K will introduce an uncertainty of $\sim 10\%$ in the opposite sense in absolute calibration at 2 atmospheres; i.e., if $T_{sbr} = 240$ K, the corrected antenna temperature ΔT_a^* will be underestimated by $\sim 10\%$ at an elevation of 30°. Although a conservative estimate of the uncertainties in our CS calibrations would be $\sim 20\%$, we note that basic receiver and antenna parameters are in good agreement with the $\lambda \sim 6$ mm parameters deduced by Linke and Goldsmith (1980). Line intensities are also in excellent agreement. For the $J=1-0$ line our calibrator source DR 21(OH) yielded a value of $\Delta T_a^* = 4.0 \pm 0.2$ K for the peak line intensity. This is to be compared with the value of 4.4 ± 0.4 K obtained by Linke and Goldsmith. For the $J=2-1$ line the peak intensity of $\Delta T_a^* = 4.7 \pm 0.2$ K is somewhat higher than the value 4.3 ± 0.2 K obtained by Linke and Goldsmith using the Bell Telephone Laboratories (BTL) 7 m antenna. However, for this line they used 250 kHz filters versus our 100 kHz filters which probably resulted in some underresolving of the line in their case. Their beamwidth was also larger for the $J=2-1$ line.

iii) CO

Our $J=1-0$ observations of CO and ^{13}CO were obtained using the 4.9 m antenna of the Millimeter Wave Observatory[4] (MWO) near Fort Davis, Texas. The receiver consisted of a room-temperature mixer with a double-sideband temperature of 1230 K at CO and 960 K at ^{13}CO. Calibration is considerably more complicated at CO

[3]The National Radio Astronomy Observatory is operated by Associated Universities, Inc. under contract to the National Science Foundation.

frequencies as the atmospheric opacities are substantially different in the signal and image sidebands. An image rejection filter was also unavailable during our observations so that antenna and receiver parameters could not be reliably estimated. We instead made use of an empirically determined T_c curve (Loren 1979) to scale our observations which were conducted in the double-sideband mode with chopper wheel calibrations. In addition, we monitored "calibration" sources whose absolute intensities are well determined (or agreed upon) from observations at Kitt Peak and Fort Davis (cf. Ulich and Haas 1976). These calibration sources were interspersed with our sources at various elevation angles to ensure repeatability and reasonably reliable calibrations. The spectrometer at MWO consisted of 2 filter banks: 128×250 kHz and 128×62.5 kHz, operating in parallel. The spectral resolutions were therefore 0.65 and 0.16 km s^{-1} at CO and 0.68 and 0.17 km s^{-1} at ^{13}CO. The antenna beam width at CO frequencies is ~2.'3 (Loren 1979).

The observing technique was frequency switching, with overlap switching to enhance signal-to-noise whenever the line widths were sufficiently narrow to permit this mode of operation.

b) *Observations*

Table 1 summarizes the observational parameters. Our sources are drawn from the list of ultracompact H II regions associated with OH masers that were investigated by Habing *et al.* (1974), and Israel, Habing, and de Jong (1973). The coordinates, distances D, and sizes of the radio condensations d, are listed in Table 2 along with references. We have also included in our investigations a few H_2O maser sources associated with star formation regions (Lo, Burke, and Haschick 1975; Morris and Knapp 1976). The exact relationships between H_2O masers and compact H II regions are unclear. They are often found to be spatially associated but not coincident with radio condensations (Forster, Welch, and Wright 1978). Lo, Burke, and Haschick (1975) have suggested that the poor correlation with continuum emission may be due to the fact that H_2O maser sources represent an earlier stage in the evolution of H II regions as compared to OH masers.

Tables 3, 4, and 5 present our observations of NH_3, CS, and CO. The reported values of ΔT_a^* the antenna temperature corrected to the top of the atmosphere, V_r the velocity of the peak of the emission lines relative to the local standard of rest, and ΔV_r the FWHM line width uncorrected for filter broadening, were determined from Gaussian fits to the data in the case of NH_3 and CS. Quoted errors are the 1 σ errors from the fits. Because of the fitting over the line profile, parameters are determined to better than the dispersion in individual frequency channels. For CO line profiles, Gaussian fits are probably not justified. Hence line parameters are simply measured from the line profiles. We estimate an rms uncertainty in ΔT_a^* of 0.8 K and 0.2 K, respectively, for CO and ^{13}CO. Uncertainties for V_r and ΔV_r are estimated to be on the order of a channel width ~0.7 km s^{-1}. Figures 1*a*–1*j* present our NH_3 mapping results in the form of contour diagrams. Here we have plotted peak values of ΔT_a^* for the main quadrupole hyperfine component of the $(J, K)=(1,1)$ transition. Figures 2*a* and 2*b* present CS mapping results of NGC 7538 in the $J=1-0$ and $J=2-1$ lines.

c) *Analysis*

We have analyzed our NH_3 data as described by Barrett, Ho, and Myers (1977). We first consider the NH_3 data obtained at Haystack with a 1.'4 beam. These represent the most extensive and complete set of data we have, from

[4]The Millimeter Wave Observatory is operated by the Electrical Engineering Research Laboratory of the University of Texas at Austin, with support from the National Science Foundation, and the MacDonald Observatory.

TABLE 1

OBSERVATIONAL PARAMETERS

Molecule	Transition	Frequency (MHz)	Telescope	Beam Size	Spectral Resolution (km s^{-1})	Receiver	T_{sys}* (K)[a]
NH_3 ...	$(J, K)=(1,1)$	23694.495	Haystack 36.6 m	1.'4	2.1, 0.21	Maser	440–660
			MPIfR 100 m	43″	0.80	Paramp	500
	$(J, K)=(2,2)$	23722.633	Haystack 36.6 m	1.'4	2.1, 0.21	Maser	440–660
			MPIfR 100 m	43″	0.80	Paramp	500
CS.....	$J=1-0$	48991.00	NRAO 11 m	2.'7	0.61, 0.18	Cooled Mixer	984
	$J=2-1$	97981.01	NRAO 11 m	1.'5	0.31, 0.092	Cooled Mixer	814
CO.....	$J=1-0$	115271.20	MWO 4.9 m	2.'3	0.65, 0.16	Mixer	4000
^{13}CO ...	$J=1-0$	110201.37	MWO 4.9 m	2.'3	0.68, 0.17	Mixer	2100

[a]$T_{sys}^* = T_{sys}/G_s\eta_b e^{-\tau_z}$ is the effective system temperature outside of the atmosphere.

TABLE 2

LIST OF UCHII REGIONS

Source	R. A. (1950)	Decl. (1950)	Type of Region	D (kpc)	d (pc)	Reference
S235 AB	$05^h37^m31^s.5$	35°41′24″	CHII, H_2O, IR	2.1	0.6	1–5
S255	06 09 58.0	18 00 02	CHII, H_2O, OH, IR	1.5	<0.4	3,5–10
OH 10.6−0.4 ...	18 07 30.6	−19 56 31	UCHII, H_2O, OH, IR	6.0[a]	<0.13	5,7,11–14
W33 B	18 10 59.6	−18 02 47	UCHII, H_2O, OH	6.6	<0.02	5,7,11, 16–17
W33 A	18 11 44.6	−17 52 57	H_2O, OH, IR	4.4	···	5,11,15–18, 19
OH 69.5−1.0 ...	20 08 09.8	31 22 41	UCHII, H_2O, OH	3.5[a]	<0.02	5,11,20
W75 N	20 36 50.0	42 26 58	UCHII, H_2O, OH, IR	3.0	<0.06	5,11,12, 21–23
S140	22 17 41.0	63 03 00	UCHII, H_2O, IR	1.0	0.02	5,9,24–27
S156 A	23 03 04.6	59 58 29	UCHII	3.5	~0.1–0.3	3,28,32
NGC 7538	23 11 36.5	61 11 49	UCHII, H_2O, IR	3.5	<0.03	5,11,25, 28–31

[a] Distances are unknown. These are adopted distances from the references cited.

REFERENCES FOR TABLE 2.—(1) Israel and Felli 1978. (2) Glushkov, Denisyuk, and Karyagina 1975. (3) Lo, Burke, and Haschick 1975. (4) Sibille, Lunel, and Bergeat 1976. (5) Genzel and Downes 1977. (6) Israel 1976. (7) Knowles, Caswell, and Goss 1976. (8) Pipher and Soifer 1976. (9) Beichman, Becklin, and Wynn-Williams 1979. (10) Evans, Blair, and Beckwith 1977. (11) Habing *et al.* 1974. (12) Matthews *et al.* 1977. (13) Fazio *et al.* 1978. (14) Goss *et al.* 1973. (15) Dyck and Capps 1978. (16) Goss, Matthews, and Winnberg 1978. (17) Wynn-Williams, Werner, and Wilson 1974. (18) Dyck and Simon 1977. (19) Evans *et al.* 1979. (20) Downes *et al.* 1979. (21) Harvey, Campbell, and Hoffmann 1977. (22) Harris 1975. (23) Dickel, Dickel, and Wilson 1978. (24) Morris and Knapp 1976. (25) Knapp *et al.* 1976. (26) Harvey, Campbell, and Hoffman 1978. (27) Blair *et al.* 1977. (28) Israel, Habing, and de Jong 1973. (29) Beetz *et al.* 1976. (30) Wynn-Williams, Becklin, and Neugebauer 1974. (31) Downes and Wilson 1974. (32) Israel 1977.

which we will attempt to deduce bulk physical properties for the detected clouds as a class. For the position in each source where we have both (1,1) and (2,2) data, we have computed the optical depth $\tau_m(1,1)$ for the main quadrupole hyperfine component. These values are in general representative of these regions. From the observed values of ΔT_a^* and the deduced values of τ_m we derive the excitation temperatures $T_{ex}(1,1)$ as follows:

$$J_\nu[T_{ex}(1,1)] = J_\nu(T_b) + \frac{\Delta T_a^*}{[1-e^{-\tau_m}]\Phi}, \tag{1}$$

where $J_\nu(T) = T_0[e^{T_0/T}-1]^{-1}$ is the intensity of the radiation in units of temperature, $T_0 = h\nu/k$, and T_b is the background temperature taken to be 2.8 K. A lower limit to $T_{ex}(1,1)$ is thus obtained by assuming beam filling factor $\Phi = 1$. A rotational temperature $T_R(2-1)$ reflecting the relative populations in the (1,1) and (2,2) levels can be obtained from the ratio $\Delta T_a^*(2,2)/\Delta T_a^*(1,1)$. Although the moderate optical depths of the (1,1) line are taken into account, numerous assumptions enter into the calculation of $T_R(2-1)$. This is discussed in some detail by Ho *et al.* (1979). Nevertheless, as we will discuss below, the derived values of $T_R(2-1)$ can be related to the kinetic temperature T_k as deduced from CO. We find the empirical relationship $T_R(2-1)/T_k = 0.7 \pm 0.1$. From the deduced values of T_{ex} and $T_R(2-1)$, an estimate of the density $n(H_2)$ can be obtained from a two-level excitation model of the NH_3 inversion doublet,

$$n(H_2) = \frac{A_{1-0}}{C_{1-0}}\left[\frac{J_\nu(T_{ex})-J_\nu(T_b)}{J_\nu(T_k)-J_\nu(T_{ex})}\right]\left[1+\frac{J_\nu(T_k)}{T_0}\right], \tag{2}$$

where A_{1-0} is the Einstein A coefficient, C_{1-0} is the collision rate, and T_k is assumed to be $T_R(2-1)/0.7$.

TABLE 3A

OBSERVED NH_3 (1, 1) LINE PARAMETERS TOWARD UCHII REGIONS AT HAYSTACK

SOURCE	POSITION $\Delta\alpha, \Delta\delta$ 1'.5, 1'.5	$\Delta V_{res} = 2.11$ km s^{-1} ΔT_{rms} (K)	ΔT_a^* (K)	$\delta(\Delta T)$ (K)	V_r (km s^{-1})	$\delta(V_r)$ (km s^{-1})	ΔV (km s^{-1})	$\delta(\Delta V)$ (km s^{-1})	$\Delta V_{res} = 0.206$ km s^{-1} ΔT_{rms} (K)	ΔT_a^* (K)	$\delta(\Delta T)$ (K)	V_r (km s^{-1})	$\delta(V_r)$ (km s^{-1})	ΔV (km s^{-1})	$\delta(\Delta V)$ (km s^{-1})
S235 AB	(0,1)	0.06	<0.16	...	...	...	...	...	0.22	<0.68	...	...	...	...	...
	(0,0)	0.05	0.40	0.08	−16.9	0.2	2.2	0.5	0.24	0.56	0.12	−17.0	0.3	1.6	0.7
	(0,−1)	0.06	0.60	0.08	−16.6	0.2	2.9	0.4	0.26	0.76	0.12	−17.0	0.2	1.8	0.4
	(0,−2)	0.06	<0.20	...	...	...	...	...	0.27	<0.80	...	...	...	...	...
	(1,0)	0.06	<0.28	...	...	...	...	...	0.28	<0.84	...	...	...	...	...
	(1,−1)	0.06	<0.16	...	...	...	...	...	0.26	<0.80	...	...	...	...	...
	(−1,0)	0.07	<0.20	...	...	...	...	...	0.32	<0.96	...	...	...	...	...
	(−1,−1)	0.06	<0.16	...	...	...	...	...	0.25	<0.76	...	...	...	...	...
S255	(0,2)	0.06	<0.20	...	...	...	...	...	0.28	<0.84	...	...	...	...	...
	(0,1)	0.06	0.60	0.08	8.7	0.2	3.5	0.5	0.26	0.64	0.12	8.3	0.2	2.3	0.5
	(0,0)	0.04	0.36	0.04	7.0	0.1	2.9	0.3	0.20	0.44	0.08	7.2	0.2	2.3	0.6
	(0,−1)	0.03	0.48	0.08	6.6	0.3	3.0	0.7	0.15	0.68	0.08	6.6	0.1	1.6	0.2
	(0,−2)	0.07	<0.20	...	...	...	...	...	0.32	<0.96	...	...	...	...	...
	(1,0)	0.07	<0.20	...	...	...	...	...	0.30	<0.92	...	...	...	...	...
	(−1,0)	0.07	<0.20	...	...	...	...	...	0.32	<0.96	...	...	...	...	...
OH 10.6	(0,1)	0.10	<0.32	...	...	...	...	...	0.42	<1.24	...	...	...	...	...
	(0,0)	0.04	1.04	0.08	−3.1	0.2	5.5	0.4	0.18	1.16	0.08	−2.9	0.2	4.5	0.4
	(0,−1)	0.10	<.32	...	...	...	...	...	0.45	<1.36	...	...	...	...	...
	(1,0)	0.04	0.64	0.08	−2.5	0.2	3.3	0.5	0.18	0.76	0.08	−2.7	0.2	3.1	0.5
	(−1,0)	0.07	0.52	0.08	−3.1	0.4	6.6	1.1	...	...	...	...	...	...	...
W33 B	(0,1)	0.10	<0.28	...	...	...	...	...	0.38	<1.16	...	...	...	...	...
	(0,0)	0.10	1.32	0.16	55.3	0.3	4.3	0.6	0.45	1.56	0.24	55.7	0.2	2.6	0.5
	(0,−1)	0.08	0.36	0.08	56.6	0.5	4.4	1.2	0.36	0.44?	0.08	56.8	0.8	6.8	1.8
	(1,0)	0.06	<0.32	...	...	...	...	...	0.28	<1.00	...	...	...	...	...
	(−1,0)	0.05	0.72	0.12	54.4	0.3	3.9	0.7	0.23	0.80	0.08	54.3	0.2	3.1	0.4
W33 A	(0,1)	0.08	1.52	0.48	35.2	1.1	6.7	3.6	0.37	1.44	0.16	34.9	0.4	5.9	0.9
	(0,0)	0.05	2.32	0.28	36.5	0.3	5.2	0.9	0.29	2.40	0.20	36.4	0.2	5.3	0.6
	(0,−1)	0.08	1.12	0.12	34.8	0.3	5.4	0.8	0.38	0.88	0.12	35.1	0.4	6.1	0.9
	(1,0)	0.04	0.88	0.08	35.3	0.3	6.4	1.0	0.29	1.16	0.08	35.2	0.2	4.2	0.4
	(−1,1)	0.06	0.56	0.20	35.7	0.7	4.3	1.7	0.26	0.72	0.20	35.9	0.4	3.1	0.9
	(−1,0)	0.05	2.12	0.20	36.4	0.2	4.2	0.5	0.34	2.52	0.20	36.5	0.1	2.8	0.2
	(−1,−1)	0.05	1.24	0.16	36.1	0.3	4.3	0.6	0.32	1.28	0.16	36.0	0.2	3.8	0.5
	(−2,0)	0.08	0.96	0.12	36.4	0.2	3.4	0.4	0.34	1.20	0.24	36.0	0.3	2.6	0.6
OH 69.5	$(0,\frac{1}{2})$	0.06	0.96	0.08	10.7	0.2	3.8	0.4	...	...	...	...	...	...	...
	(0,0)	0.08	1.24	0.12	11.4	0.2	3.9	0.5	...	...	...	...	...	...	...
	$(0,-\frac{1}{2})$	0.06	0.80	0.04	11.3	0.1	3.0	0.2	...	...	...	...	...	...	...
	$(\frac{1}{2},0)$	0.06	0.72	0.20	11.1	0.4	2.9	0.9	...	...	...	...	...	...	...
	$(-\frac{1}{2},0)$	0.05	1.00	0.08	11.6	0.2	3.9	0.4	...	...	...	...	...	...	...

TABLE 3A—*Continued*

OBSERVED NH_3 (1, 1) LINE PARAMETERS TOWARD UCHII REGIONS AT HAYSTACK

SOURCE	POSITION $\Delta\alpha, \Delta\delta$ 1:5, 1:5	$\Delta V_{res} = 2.11$ km s^{-1} ΔT_{rms} (K)	ΔT_a^* (K)	$\delta(\Delta T)$ (K)	V_r (km s^{-1})	$\delta(V_r)$ (km s^{-1})	ΔV (km s^{-1})	$\delta(\Delta V)$ (km s^{-1})	$\Delta V_{res} = 0.206$ km s^{-1} ΔT_{rms} (K)	ΔT_a^* (K)	$\delta(\Delta T)$ (K)	V_r (km s^{-1})	$\delta(V_r)$ (km s^{-1})	ΔV (km s^{-1})	$\delta(\Delta V)$ (km s^{-1})
W75 N	(0,1)	0.05	0.40	0.04	9.2	0.2	4.4	0.6	...	...	...	...	...	...	...
	(0,0)	0.12	1.40	0.20	9.6	0.4	6.7	1.2	...	...	...	...	...	...	...
	(0,−1)	0.09	<0.28	...	...	...	...	...	...	...	...	...	...	...	...
	(1,0)	0.06	0.36	0.08	9.0	0.4	3.2	0.9	...	...	...	...	...	...	...
	(−1,0)	0.08	0.40	0.12	9.5	0.6	4.6	1.6	...	...	...	...	...	...	...
S140	(0,1)	0.06	0.84	0.24	−7.3	0.3	2.3	0.7	0.30	1.04	0.12	−7.2	0.1	1.9	0.3
	(0,0)	0.08	0.72	0.16	−7.2	0.3	3.4	0.8	0.36	0.76	0.16	−7.4	0.3	2.9	0.7
	(1,2)	0.06	0.60	0.08	−7.4	0.2	2.7	0.4	0.28	1.04	0.24	−7.5	0.2	1.9	0.5
	(1,1)	0.07	1.48	0.16	−6.7	0.1	2.4	0.3	0.27	2.68	0.16	−6.9	0.0	1.5	0.1
S140	(1,0)	0.08	0.40	0.24	−7.1	0.7	2.2	1.7	...	...	...	...	...	...	...
	(−1,1)	0.05	0.20	0.08	−7.6	0.5	2.3	1.2	0.24	<0.72	...	...	...	...	...
	(2,1)	0.06	0.44	0.12	−7.2	0.3	...	...	0.27	<0.80	...	...	...	...	...
NGC 7538	(0,1)	0.08	<0.24	...	...	...	...	...	...	...	...	...	...	...	...
	(0,0)	0.11	1.20	0.12	−57.6	0.2	4.3	0.5	...	...	...	...	...	...	...
	(0,−1)	0.06	1.52	0.12	−56.4	0.2	4.8	0.5	...	...	...	...	...	...	...
	(0,−2)	0.08	<0.28	...	...	...	...	...	...	...	...	...	...	...	...
	(1,0)	0.06	0.40	0.04	−56.1	0.2	5.2	0.5	...	...	...	...	...	...	...
	(1,−1)	0.06	0.88	0.16	−56.4	0.4	4.7	1.0	...	...	...	...	...	...	...
	(−1,0)	0.06	0.24	0.12	−57.2	1.3	4.6	3.4	...	...	...	...	...	...	...
	(−1,−1)	0.06	0.32	0.12	−55.9	1.0	5.8	2.4	...	...	...	...	...	...	...
S156 A	(0,1)	0.05	0.20	0.12	−50.6	0.6	1.8	1.4	0.22	<0.68	...	...	...	...	...
	(0,0)	0.04	0.36	0.04	−52.1	0.2	3.2	0.4	0.19	0.40	0.08	−53.0	0.3	3.4	0.6
	(0,−1)	0.05	<0.16	...	...	...	...	...	0.22	<0.68	...	...	...	...	...
	(1,0)	0.04	0.32	0.04	−52.5	0.2	3.0	0.4	0.18	0.52	0.12	−52.4	0.3	1.9	0.6
	(−1,0)	0.04	0.20	0.04	−52.5	0.3	3.4	0.8	0.21	0.32	0.16	−53.4	0.5	1.4	1.2

TABLE 3B

OBSERVED NH_3 (2, 2) LINE PARAMETERS TOWARD UCHII REGIONS AT HAYSTACK

SOURCE	POSITION $(\Delta\alpha, \Delta\delta)$ (1:5, 1:5)	$\Delta V_{res} = 2.11$ km s^{-1} ΔT_{rms} (K)	ΔT_a^* (K)	$\delta(\Delta T)$ (K)	V_r (km s^{-1})	$\delta(V_r)$ (km s^{-1})	ΔV (km s^{-1})	$\delta(\Delta V)$ (km s^{-1})	$\Delta V_{res} = 0.206$ km s^{-1} ΔT_{rms} (K)	ΔT_a^* (K)	$\delta(\Delta T)$ (K)	V_r (km s^{-1})	$\delta(V_r)$ (km s^{-1})	ΔV (km s^{-1})	$\delta(\Delta V)$ (km s^{-1})
S235 AB	(0,0)	0.04	0.20	0.08	−16.4	1.1	6.1	2.5	0.21	<0.64	...	...	...	...	...
S255	(0,0)	0.05	0.32	0.04	7.4	0.2	2.6	0.4	0.24	<0.72	...	...	...	...	...
OH 10.6	(0,0)	0.08	0.68	0.08	−3.6	0.3	5.4	0.6	0.34	0.60	0.12	−3.9	0.5	5.5	1.1
W33 B	(0,0)	0.07	0.56	0.16	55.9	0.6	4.4	1.4	0.30	0.72	0.12	55.8	0.3	2.7	0.6
W33 A	(0,0)	0.08	1.04	0.04	36.5	0.1	3.8	0.3	0.35	1.12	0.12	36.0	0.2	3.6	0.4
OH 69.5	(0,0)	0.04	0.64	0.08	11.0	0.2	3.9	0.6	...	...	...	...	...	...	...
W75 N	(0,0)	0.06	0.84	0.28	9.1	0.5	3.4	1.3	...	...	...	...	...	...	...
S140	(0,1)	0.04	0.52	0.04	−6.9	0.1	2.6	0.3	0.18	0.72	0.12	−7.1	0.2	1.8	0.4
NGC 7538	(0,−1)	0.05	0.76	0.04	−56.6	0.2	4.1	0.4	...	...	...	...	...	...	...
S156 A	(0,0)	0.04	0.16?	...	...	...	...	...	0.19	<0.56	...	...	...	...	...

TABLE 3C

OBSERVED AND DERIVED NH_3 LINE PARAMETERS TOWARD UCHII REGIONS AT EFFELSBERG

Source	Position ($\Delta\alpha, \Delta\delta$) (40″,40″)	$(J,K)=(1,1)$ ΔT_a^* (K)	ΔT_{rms} (K)	V_r^1 (km s^{-1})	ΔV_r (km s^{-1})	$(J,K)=(2,2)$ ΔT_a^* (K)	ΔT_{rms} (K)	V_r^1 (km s^{-1})	$\Phi=1$ ΔV_r (km s^{-1})	$\tau_m(1,1)$	T_{ex} (K)	$T_R(2-1)$ (K)
OH 10.6	(0,0)	3.8	0.6	−3.7	5.3	2.7	0.8	−4.1	7.0	0.4	13.7	25^{+11}_{-6}
W33 B	(0,0)	3.0	0.5	55.7	3.3	2.5	0.4	55.7	2.9	2.4	6.1	$23^{+\infty}_{-6}$
W33 A	(0,0)	6.0	0.5	36.2	4.5	3.9	0.5	36.5	4.5	1.9	9.9	20^{+4}_{-3}
OH 69.5	(0,0)	2.5	0.2	11.8	3.8	1.6	0.3	11.4	2.7	1.7	5.9	20^{+5}_{-3}
	(0,1)	2.9	0.3	11.0	3.9	1.7	0.3	11.8	4.5	2.0	6.2	18^{+4}_{-3}
W75 N	(0,0)	2.4	0.3	9.6	1.7	2.0	0.3	9.7	2.4	0.4	10.3	28^{+8}_{-5}
	(1,0)	2.3	0.3	8.8	2.2	1.2	0.3	9.3	2.8	∼0.2	∼16.0	21^{+5}_{-4}
	(2,0)	0.9	0.3	9.5	2.4	1.0	0.3	10.0	0.5	∼0.3	∼6.8	36^{+102}_{-14}
NGC 7538 ...	(0,0)	1.5	0.3	−56.9	2.6	1.3	0.2	−57.2	3.0	0.8	5.5	28^{+19}_{-7}
	(0,1)	<0.4	...	...	...	<0.6	...	...	...	...	...	...
	(0,−1)	2.4	0.4	−57.0	2.8	1.9	0.4	−56.7	2.0	≲1.0	≳6.6	25^{+16}_{-6}
	(0,−2)	3.1	0.3	−56.0	4.9	2.1	0.4	−55.9	4.9	1.4	6.9	21^{+6}_{-4}
	(0,−3)	1.4	0.3	−56.2	3.6	1.1	0.3	−56.2	1.6	0.8	5.4	26^{+23}_{-7}
	(1,−2)	4.0	0.5	−56.3	2.8	2.3	0.5	−55.7	3.7	0.4	14.3	22^{+5}_{-4}
	(−1,−2)	2.3	0.3	−56.6	2.6	1.3	0.3	−56.1	3.8	<2.0	>5.5	18^{+6}_{-3}

[1]Velocity resolution was 0.80 km s^{-1}.

As the NH_3 emission regions are observed to be small, and as clumping of the NH_3 molecules may occur (Barrett, Ho, and Myers 1977; Schwartz *et al.* 1977; Ho *et al.* 1979), we also calculated values for T_{ex} and $n(H_2)$ for the case $\Phi=0.1$. This was not always possible, as there is a minimum value of the filling factor Φ_{min} for which $T_{ex}=T_k$. In order to see how reasonable the assumption $\Phi=0.1$ would be, we have also calculated Φ_{min} for all of the sources. We find that for the majority of the sources in fact $\Phi_{min}\sim 0.1$. The values are given in Table 6.

Having an estimate of $n(H_2)$, we then computed the total mass of the associated cloud from the observed sizescale of the emission region (diameter$=2R$). For a Gaussian density distribution, the mass $M=(\pi/\ln 2)^{3/2}\rho_{max}R^3$, where ρ_{max} is the peak mass density and R is the half-width at half-maximum. Hence in more convenient units,

$$\frac{M}{M_\odot}=116\left[\frac{R'}{1'.0}\right]^3\left[\frac{D}{1\text{ kpc}}\right]^3\left[\frac{n(H_2)}{10^4\text{ cm}^{-3}}\right], \tag{3}$$

where D is the distance, and R' is the radius of the emission region corrected for beam broadening assuming a Gaussian antenna beam and a Gaussian source distribution. We have assumed our deduced values of $n(H_2)$ which is beam-averaged to be the actual peak density. This underestimate is less than 30% as long as $R'\gtrsim 1'.5$. For substantially smaller values of R', underestimates of ρ_{max} are corrected for through the parameter Φ. We have computed M for both the $\Phi=1$ and $\Phi=0.1$ cases. Note that for $\Phi=0.1$, R' is taken to be $0.7'\,[\Phi/(1-\Phi)]^{1/2}\sim 14''.0$. We also calculated the critical masses M_c for gravitational stability using the virial theorem. Balancing the thermal and gravitational energy, we obtain

$$\frac{M_c}{M_\odot}=\frac{1}{M_\odot}\left[\frac{3kT_k}{Gn(H_2)^{1/3}m_{H_2}{}^{4/3}}\right]^{3/2}=20.0\left[\frac{T_k}{20}\right]^{3/2}\left[\frac{n(H_2)}{10^4}\right]^{-1/2}. \tag{4}$$

The observed or calculated values of τ_m, R, T_{ex} for $\Phi=1$, $T_R(2-1)$, $n(H_2)$, and M for $\Phi=1$ and $\Phi=0.1$, Φ_{min}, and M_c are summarized in Table 6.

Additional NH_3 observations were conducted at Effelsberg with a 43″ beam in order to assess the importance of the beam filling factor Φ in the analysis of the Haystack data. We have analyzed these data in the same manner as described above, obtaining values for ΔT_a^*, τ_m, T_{ex} for the case of $\Phi=1$ with respect to the Effelsberg beam, and also $T_R(2-1)$. These values are given in Table 3*c*. For the six sources for which we have data at both telescopes, we compare the values of ΔT_a^* in Figure 3. Because of the different beam sizes, we compare only those positions where both

TABLE 4

OBSERVED CS LINE PARAMETERS TOWARD UCHII REGIONS

Source	Position ($\Delta\alpha, \Delta\delta$) (1'.5 1'.5)	$J=1-0$, $\Delta V_{res}=0.18$ km s^{-1}						$J=2-1$, $\Delta V_{res}=0.31$ km s^{-1}					
		ΔT_a^* (K)	$\delta(\Delta T)$ (K)	V_r (km s^{-1})	$\delta(V_r)$ (km s^{-1})	ΔV (km s^{-1})	$\delta(\Delta V)$ (km s^{-1})	ΔT_a^* (K)	$\delta(\Delta T)$ (K)	V_r (km s^{-1})	$\delta(V_r)$ (km s^{-1})	ΔV (km s^{-1})	$\delta(\Delta V)$ (km s^{-1})
W33 B	(0,1)	<0.4	...	...	...	...	...	<0.5	...	...	...	...	...
	(0,1/2)	...	...	...	...	...	...	0.52	0.11	57.47	0.31	2.88	0.89
	(0,0)	0.42	0.07	56.0	0.43	8.20	1.16	0.70	0.10	57.75	0.06	1.72	0.18
	(0,−1/2)	...	...	...	...	...	...	<0.5	...	...	...	...	...
	(0,−1)	≲0.5[a]	...	(56)	...	(9.8)	...	<0.5	...	...	...	...	...
	(1/2,0)	...	...	...	...	...	...	0.69	0.19	57.50	0.09	1.35	0.28
	(1,0)	<0.6	...	...	...	...	...	<0.5	...	...	...	...	...
	(2,0)	<0.6	...	...	...	...	...	...	...	...	...	...	...
	(−1/2,0)	...	...	...	...	...	...	<0.5	...	...	...	...	...
	(−1,0)	≲0.5[a]	...	(54)	...	(4.9)	...	<0.5	...	...	...	...	...
NGC 7538.	(0,1)	1.49	0.12	−56.88	0.12	4.77	0.31	0.36	0.07	−56.85	0.34	5.94	0.95
	(0,0)	3.12	0.11	−56.76	0.04	4.10	0.08	4.21	0.08	−57.06	0.02	4.16	0.04
	(0,−1)	2.77	0.15	−56.39	0.06	4.41	0.12	3.74	0.07	−56.68	0.02	5.23	0.08
	(0,−2)	0.82	0.11	−55.78	0.24	6.00	0.67	0.65	0.07	−56.42	0.21	6.85	0.64
	(1,1)	1.30	0.16	−56.63	0.06	3.06	0.24	...	...	...	...	...	...
	(1,0)	3.17	0.10	−56.60	0.03	4.41	0.07	1.25	0.07	−56.02	0.08	4.59	0.22
	(1,−1)	2.13	0.17	−56.51	0.06	4.28	0.24	2.15	0.06	−56.97	0.04	5.27	0.11
	(2,0)	2.14	0.16	−56.39	0.06	4.28	0.24	...	...	...	...	...	...
	(−1,0)	2.06	0.12	−56.76	0.06	4.77	0.24	1.57	0.07	−57.69	0.04	3.89	0.15
	(−1,−1)	1.72	0.18	−56.57	0.06	2.94	0.24	1.55	0.07	−56.78	0.04	4.01	0.15
NGC 7538[b]	(0,0)	≲0.2	...	...	...	...	...	0.93	0.18	−57.59	0.16	2.80	0.44

[a] Line parameters were poorly determined because of signal-to-noise.
[b] $C^{34}S$ isotope observations.

TABLE 5

OBSERVED CO PARAMETERS TOWARD UCHII REGIONS

Source	Position $(\Delta\alpha, \Delta\delta)$ (3'.0, 3'.0)	^{12}CO ΔT_a^* (K)	^{12}CO V_r (km s^{-1})	^{12}CO ΔV_r (km s^{-1})	^{13}CO ΔT_a^* (K)	^{13}CO V_r (km s^{-1})	^{13}CO ΔV_r (km s^{-1})	$T_k(\Phi=0.8)$ (K)	N(CO) (10^{18}cm^{-2})
OH 10.6	(0,0)	22.0	−2.5	6.5	6.7	−2.7	5.1	31.1	7.6
	(0,1)	12.0	−2.0	5.0	...	...	...	18.5	...
	(0,−1)	9.3	−2.5	8.5	...	...	...	15.1	...
	(1,0)	10.7	−1.5	6.0	...	...	...	16.9	...
	(−1,0)	15.3	−2.5	5.0	...	...	...	22.7	...
W33 B[a].....	(0,0)	17.3	35.5	7.0	3.8	35.1	4.2	25.2	2.8
	(0,1)	18.7	34.0	4.5	...	...	...	26.9	...
	(0,−1)	12.7	34.5	6.5	...	...	...	19.4	...
	(1,0)	16.0	35.5	6.5	...	...	...	23.5	...
	(−1,0)	14.7	35.0	6.0	...	...	...	21.9	...
W33 A	(0,0)	13.3	34.0	11.0	6.0	34.4	7.7	20.2	8.3
	(0,1)	13.3	33.0	9.0	...	...	...	20.2	...
	(0,−1)	14.7	34.0	12.5	...	...	...	21.9	...
	(1,0)	10.7	36.0	10.5	...	...	...	16.9	...
	(−1,0)	14.7	34.0	10.0	...	...	...	21.9	...
OH 69.5	(0,0)	9.3	10.5	5.9	4.1	11.5	3.4	15.1	2.1
	(0,1)	6.7	10.0	5.8	...	...	...	11.8	...
	(0,−1)	12.0	11.5	4.0	...	...	...	18.5	...
	(1,0)	7.7	10.8	6.5	...	...	...	13.1	...
	(−1,0)	6.6	10.5	5.2	...	...	...	11.7	...
W75 N	(0,0)	17.6	10.5	7.8	6.2	9.8	3.2	25.6	3.9
	(0,1)	17.2	13.0	3.3	...	...	...	25.1	...
	(0,−1)	14.7	9.0	4.0	...	...	...	21.9	...
	(1,0)	16.7	10.0	5.5	...	...	...	24.4	...
	(−1,0)	6.0	9.5	9.0	...	...	...	10.9	...
S140	(0,0)	20.8	−7.5	5.3	8.6	−7.3	2.8	29.6	5.6
	(0,1)	16.3	−8.0	3.9	...	...	...	23.9	...
	(0,−1)	17.3	−8.0	4.5	...	...	...	25.2	...
	(1,0)	16.3	−8.0	5.3	...	...	...	23.9	...
	(−1,0)	15.6	−8.0	3.2	...	...	...	23.0	...
S156 A	(0,0)	18.0	−51.0	4.5	4.5	−51.8	3.3	26.1	2.8
	(0,1)	14.4	−51.0	3.9	...	...	...	21.5	...
	(0,−1)	17.3	−51.0	4.5	...	...	...	25.2	...
	(1,0)	17.6	−50.5	3.9	...	...	...	25.6	...
	(−1,0)	14.7	−51.5	3.2	...	...	...	21.9	...
NGC 7538 ..	(0,0)	21.3	−56.5	8.8	4.7	−56.5	6.0	30.2	5.8

[a] In contrast to NH_3 results, CO emission in W33 B is dominated by emission at 35 km s^{-1}. Profiles at 55–60 km s^{-1} are peculiar in appearance with the possibility of self-absorption. We estimate $T_k \lesssim 15$ K at 55–60 km s^{-1}.

telescopes were pointed at the same coordinates. These were typically the positions with the strongest emission at Haystack. Several positions off emission peaks were also observed at both telescopes. These are plotted as open circles in Figure 3. We note that peak emission positions as determined at Effelsberg may be offset from the nominal positions found at Haystack. Hence observations at Effelsberg for those sources which have not been mapped probably correspond to lower limits in emission strength and therefore density. Nevertheless, Figure 3 clearly demonstrates that observed ΔT_a^* are systematically stronger with a larger telescope. The diagonal line corresponds to the case of a very large source which fills the beam at both telescopes. The dashed lines correspond to the 1 σ uncertainties in determining ΔT_a^*.

These observed differences between the two telescopes can be used to deduce a size scale for the emission regions. We consider the effects of source geometry and size scales,

$$\Delta T_a^* = \int G(\theta, \phi) T_B(\theta, \phi) \theta \, d\theta \, d\phi, \tag{5}$$

where G is the antenna gain pattern, T_B is the brightness temperature distribution, and (θ, ϕ) are the coordinates on the sky. We assume a symmetric Gaussian beam and consider the two cases where a Gaussian and a disk distribution for

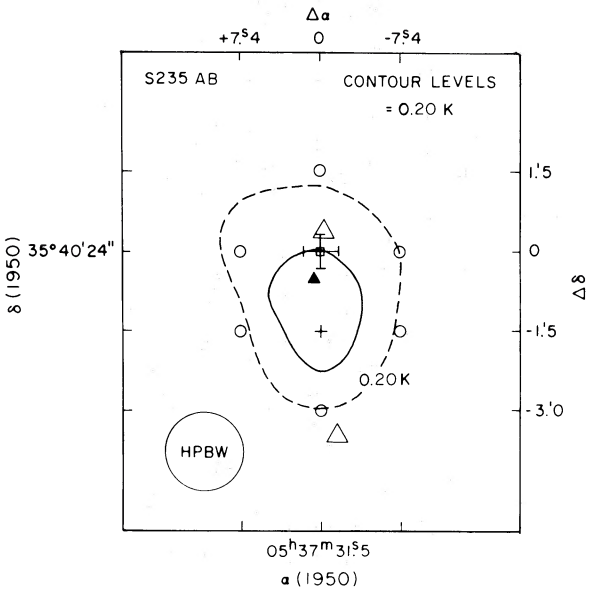

FIG. 1*a*

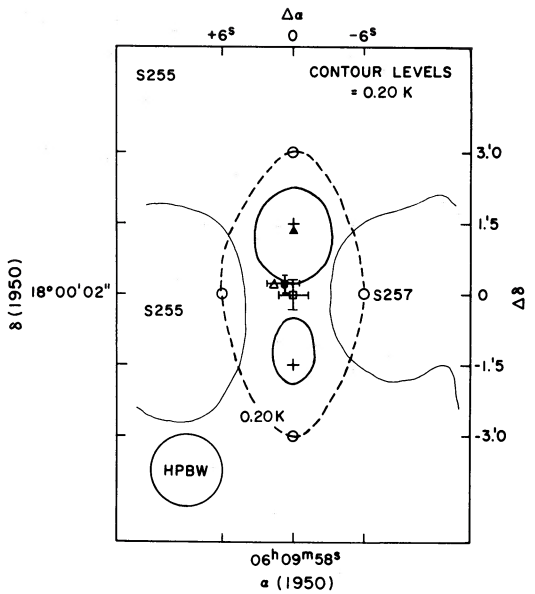

FIG. 1*b*

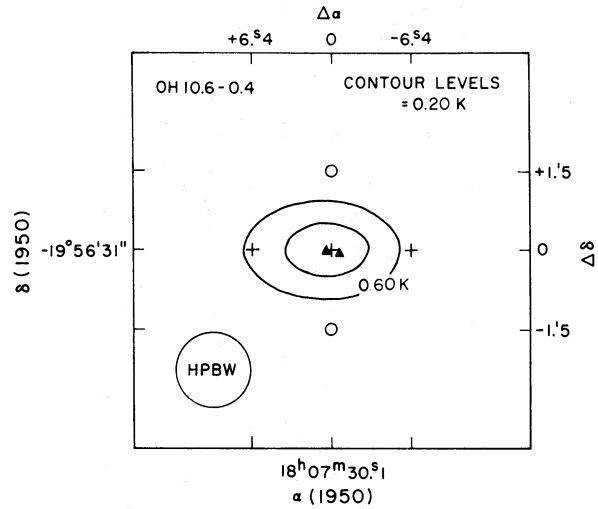

FIG. 1*c*

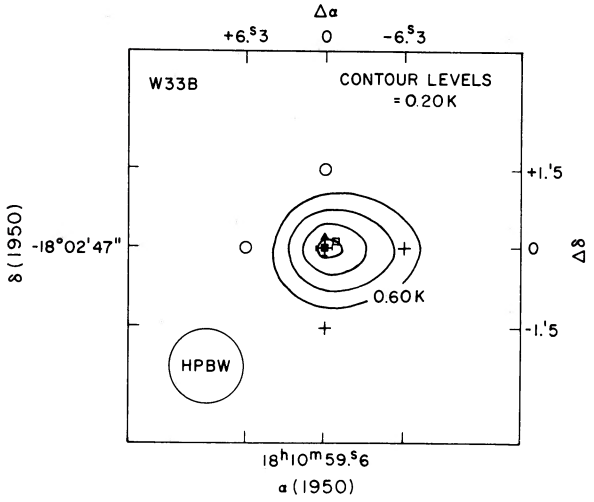

FIG. 1*d*

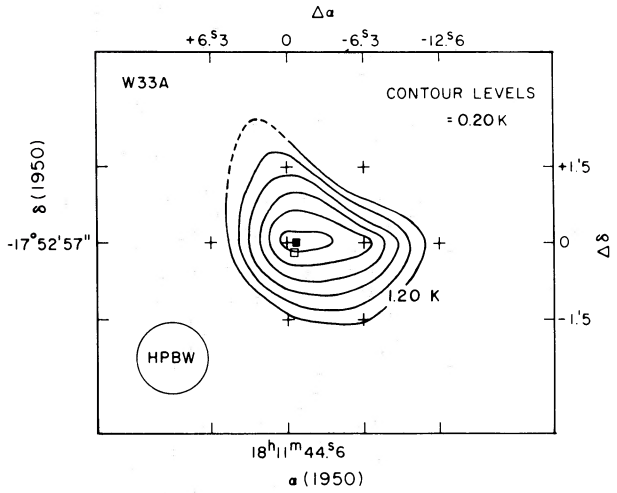

FIG. 1.—(a)–(*j*) Contour diagrams of the intensity of the main quadrupole hyperfine component of the $(J, K)=(1,1)$ emission line of NH_3 toward CHII and UCHII regions. Crosses indicate positions of observations; open circles indicate upper limits; filled triangles are UCHII regions; open triangles are CHII regions; filled squares are OH masers; open squares are H_2O masers.

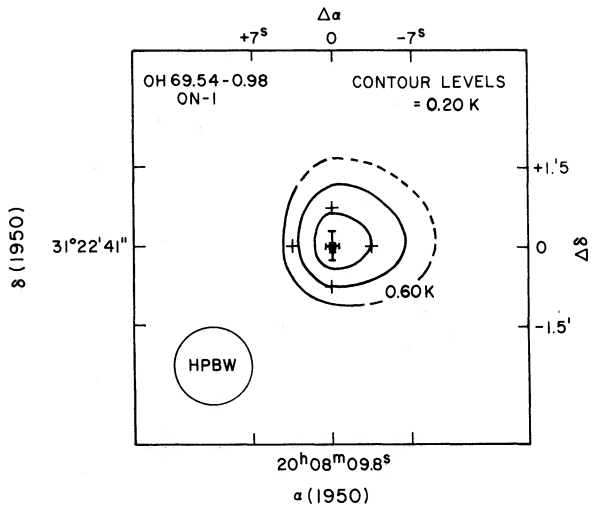

FIG. 1*f*

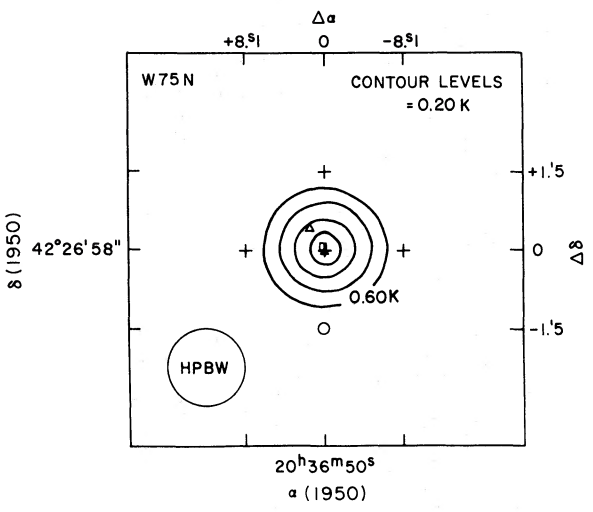

FIG. 1*g*

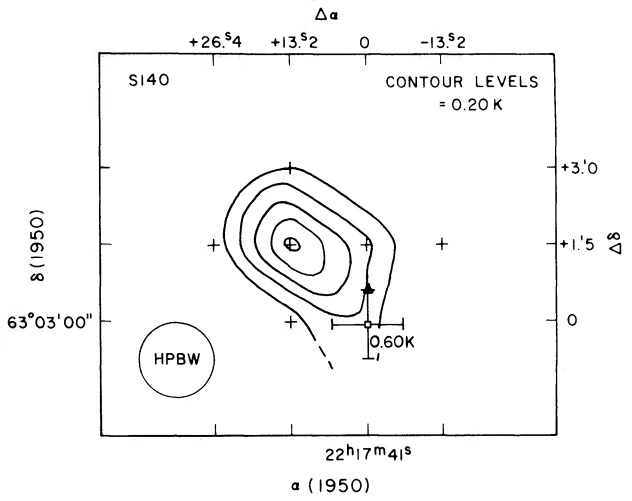

FIG. 1*h*

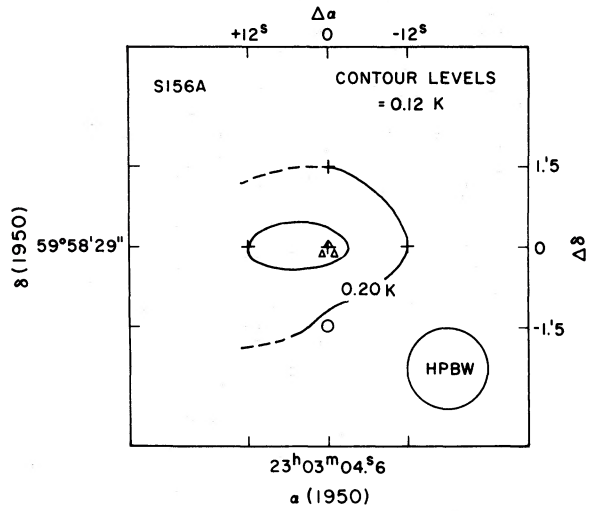

FIG. 1*i*

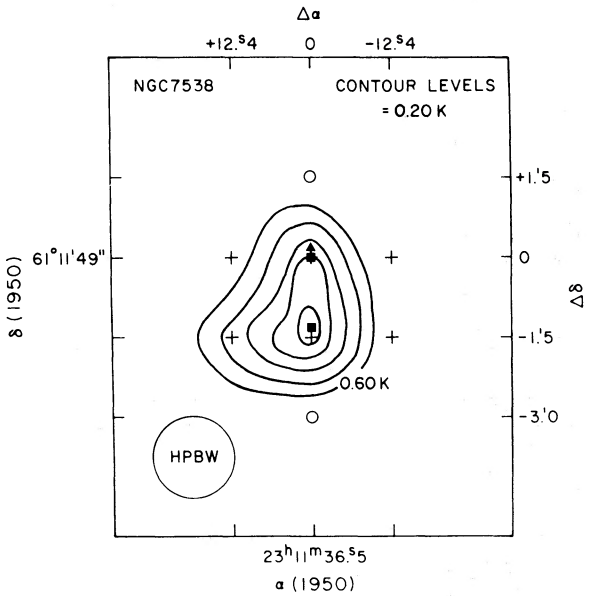

FIG. 1*j*

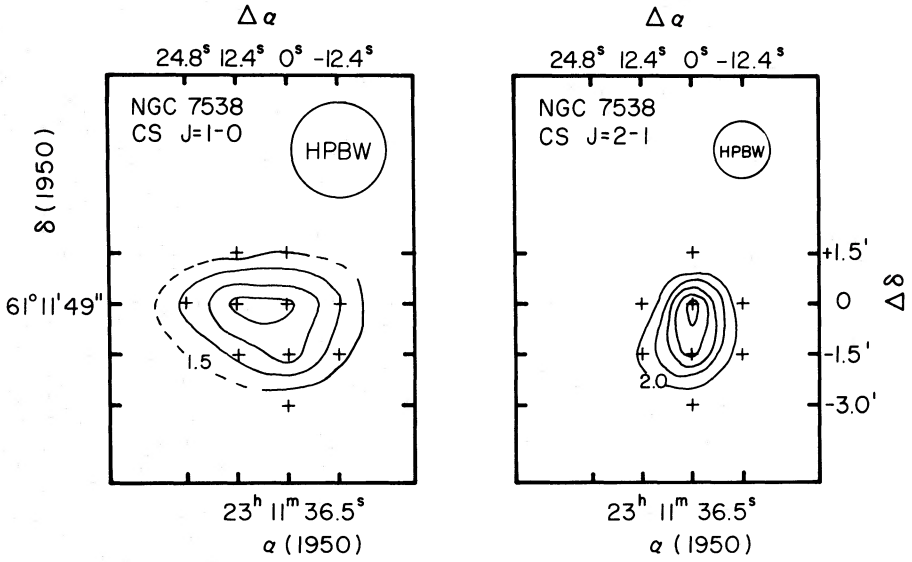

FIG. 2a FIG. 2b

FIG. 2.—Contour diagrams of the intensity of (*a*) the $J=1-0$ line and (*b*) the $J=2-1$ line of CS. Contour levels are in steps of 0.5 K. The labeled contour corresponds to 50% of the peak intensity.

T_B are centered with the antenna beam. We then obtain

$$\Delta T_a^* = A\frac{\theta_s^2}{\theta_s^2+\theta_b^2} \quad \text{(Gaussian)} \tag{6a}$$

$$= A\left[1-\exp\left(-\theta_s^2 \ln 2/\theta_b^2\right)\right] \quad \text{(disk)}, \tag{6b}$$

where A is the peak value of T_B, and θ_s and θ_b are the source and beam sizes. For two antennas of different beamwidths θ_1 and θ_2, the ratio of antenna temperatures is

$$\frac{\Delta T_a^*(\theta_1)}{\Delta T_a^*(\theta_2)} = \frac{\theta_s^2+\theta_2^2}{\theta_s^2+\theta_1^2} \quad \text{(Gaussian)} \tag{7a}$$

$$= \left[\frac{1-\exp\left(-\theta_s^2 \ln 2/\theta_1^2\right)}{1-\exp\left(-\theta_s^2 \ln 2/\theta_2^2\right)}\right] \quad \text{(disk)}. \tag{7b}$$

TABLE 6

DERIVED PHYSICAL PARAMETERS TOWARD UCHII REGIONS

Source	τ_m[a]	$\Phi=1$ T_{ex}	$T_R(2-1)$	$\Phi=1$ $n(H_2)$	$\Phi=0.1$ $n(H_2)$	Φ_{min}	$\Phi=1$ $M/M_\odot$	$\Phi=0.1$ $M/M_\odot$	$\Phi=1$ $M_c/M_\odot$	$2R$
S235 AB(0,0)	<1.2	>3.4	18^{+9}_{-5}	$>8.9\times10^2$	1.1×10^4	0.025	2.2×10^2	1.5×10^1	98	3.0
S255(0,0).....	$\lesssim0.5$	$\gtrsim3.7$	29^{+8}_{-5}	$\gtrsim1.0\times10^3$	1.3×10^4	0.024	0.8	6.4	189	1.5
OH 10.6(0,0).....	0.6	5.1	23^{+3}_{-3}	3.1×10^3	1.2×10^5	0.077	1.8×10^4	3.8×10^3	76	3.0
W33 B(0,0)	2.5	4.2	14^{+3}_{-2}	2.6×10^3	1.5×10^5	0.084	9.6×10^3	6.3×10^3	39	2.5
W33 A(0,0)	1.7	5.6	16^{+1}_{-1}	5.1×10^3	...	0.142	3.3×10^4	...	34	4.0
OH 69.5(0,0).....	1.2	4.6	18^{+3}_{-2}	2.8×10^3	1.1×10^5	0.077	3.2×10^3	6.9×10^2	55	3.0
W75 N(0,0)	1.8	4.5	19^{+10}_{-4}	2.6×10^3	7.6×10^4	0.069	3.0×10^2	3.0×10^2	62	2.0
S140 (0, 1'.5)	<0.5	>4.9	22^{+8}_{-4}	$>2.9\times10^3$	1.1×10^5	0.075	7.8×10^1	1.6×10^1	73	3.0
NGC 7538(0, −1'.5)	1.0	5.2	19^{+1}_{-1}	3.7×10^3	2.8×10^6	0.099	4.3×10^3	1.8×10^4	52	3.0
S156 A (0,0)	$\lesssim0.5$	$\gtrsim3.7$	<19?	$\gtrsim1.3\times10^3$	2.1×10^4	0.038	1.5×10^3	1.3×10^2	88	3.0

[a] τ_m and T_{ex} refer to the $(J, K)=(1,1)$ transition of NH_3.

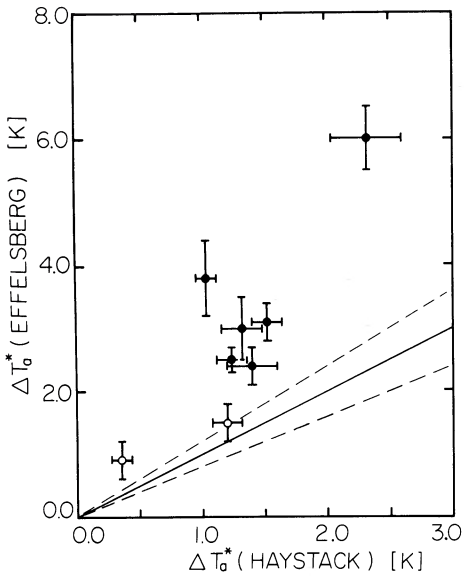

FIG. 3.—Comparison of ΔT_a^* observed at Haystack and Effelsberg. Solid line corresponds to a large source which fills the antenna beam at both telescopes. Dashed lines correspond to $\pm 20\%$ for calibration uncertainties.

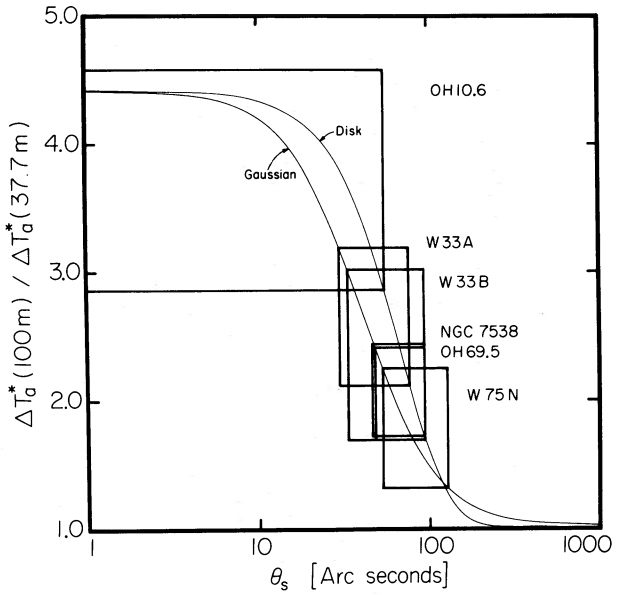

FIG. 4.—Error boxes for different emission regions as obtained from a comparison of the observations and theoretical predictions. The two curves correspond to a Gaussian and a disk source geometry.

We have plotted equation (7) in Figure 4, as well as the observed ratio of ΔT_a^* from Effelsberg and Haystack as an error box for each source. A size scale for each source is thereby implied by this analysis.

In Figure 5, we compare values of $T_R(2-1)$ as deduced at Haystack and Effelsberg. The purpose of this is to determine whether a smaller but hotter source exists in these regions which can be detected with a 43″ beam. We find that within the error bars (from the 1 σ uncertainties in determining ΔT_a^*) the observations are consistent with equal values of $T_R(2-1)$ at both telescopes for all six sources. A difference in $T_R(2-1)$ by 20 K would have been easily detectable. Hence if an embedded object exists with $T_R(2-1) \gtrsim 40$ K, its size scale must be $\lesssim 25''$. A uniform or at least relatively slow varying value of T_k (with no abrupt changes by factors of 2) is therefore implied over a range in size scales of 25″–100″ (see also Table 3C for mapping results in NGC 7538).

CO observations were obtained at Texas in order to measure the kinetic temperatures in these regions. Values of T_k are obtained from the CO observations in the usual manner:

$$T_k = T_0 \left\{ \ln \left[1 + \frac{T_0}{J_\nu(T_b) + \Delta T_a^*(^{12}\mathrm{CO})/\Phi} \right] \right\}^{-1}, \tag{8}$$

where Φ has been assumed to be 0.8 (appropriate for a source with $\theta_s \sim 5'$ and observed with the Texas antenna). We compare in Figure 6 these values of T_k with the values of $T_R(2-1)$ deduced from the NH_3 data at Haystack. We did not observe S235 AB and S255 in CO ourselves. Instead we used the data of Blair, Peters, and Vanden Bout (1975) and Evans, Blair, and Beckwith (1977). We find a good correlation between NH_3 rotational temperatures and CO kinetic temperatures: $T_R(2-1)/T_k = 0.7 \pm 0.1$. This systematically lower value of $T_R(2-1)$ for all the sources is probably due to collisions between K-ladders in NH_3 followed by rapid radiative decay from the nonmetastable states which lead to depletion of the (2,2) population relative to the (1,1) population resulting in $T_R(2-1) < T_k$ (Morris *et al.* 1973). We therefore conclude that despite the numerous assumptions which enter into the calculation of $T_R(2-1)$, the NH_3 molecule remains a good indicator of the gas temperature. We have used the empirical relation $T_k = T_R(2-1)/0.7$ in our calculations of $n(H_2)$ above instead of the actual values of T_k from CO. This is because of (1) the possibility of self-absorption effects in the CO profiles and (2) the fact that CO and NH_3 may not be coextensive so that, although the relation between $T_R(2-1)$ and T_k may hold in general, variations in individual cases may be large.

Five point maps with 3′ offsets were also obtained in order to determine the spatial variations of T_k on that size scale. In particular we were interested in whether or not the molecular clouds detected in NH_3 are well localized regions of enhanced T_k. We find from our data that except for OH 10.6 and possibly S140, T_k does not appear to be a strong peak (with enhancement by a factor of 2) on the scale of 3′. The compact nature of OH 10.6 and S140 in fact

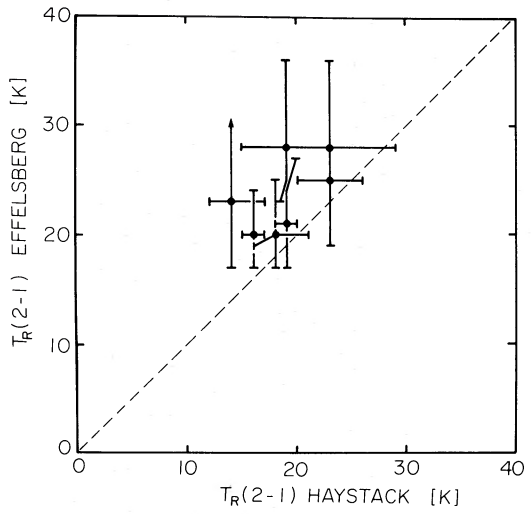

FIG. 5

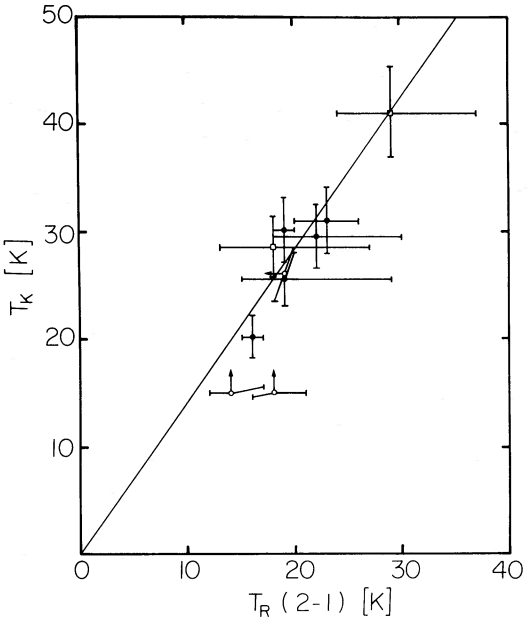

FIG. 6

FIG. 5.—Comparison of $T_R(2-1)$ as deduced independently from data at Haystack and Effelsberg. The dashed curve corresponds to equal values of $T_R(2-1)$.

FIG. 6.—A comparison of $T_R(2-1)$ as deduced from NH_3 and T_k as deduced from CO. Solid line is $T_R(2-1)/T_k = 0.7$.

have been shown by the more extensive and complete maps of Fazio *et al.* (1978) and Blair *et al.* (1977). S255, which we did not observe in CO, has also been shown (Evans, Blair, and Beckwith 1977) to be a strong peak in T_k. On the other hand, more extensive CO data of W75 N not reported here indicate a maximum in T_k with a size scale of $\sim 6'$. This may be more typical of the other sources.

Column densities for CO can be derived from ^{13}CO observations in the usual manner (Martin and Barrett 1978) by assuming the ^{13}CO transition to be thermalized, and an isotopic ratio $[CO]/[^{13}CO] = 89$:

$$N(CO) = 2.055 \times 10^{16} \left[\frac{T_k \Delta V_r}{1 - \exp(-T_0/T_k)} \right] \left\{ -\ln \left[1 - \frac{\Delta T_a^*(^{13}CO)}{\Delta T_a^*(^{12}CO)} \right] \right\}. \quad (9)$$

We note that in fact the ^{13}CO line may be moderately optically thick with subthermal excitation, in which case $N(CO)$ may be somewhat overestimated.

CS observations were obtained in order to evaluate independently the densities in these regions. Because CS is a linear molecule and the rotational levels are closely spaced, the excitation of any particular transition involves the population of many states. A multilevel statistical equilibrium calculation therefore appears unavoidable. In addition, with the possibility of large optical depths, the effects of radiative trapping must also be taken into account. Two standard approaches to the problem of radiative transfer have been the large velocity gradient model (Scoville and Solomon 1974; Goldreich and Kwan 1974) and the microturbulent model (Lucas 1976; Leung and Liszt 1976). In the case of CS, numerical solutions to the coupled equations of radiation transport and statistical equilibrium have been obtained in both models by respectively Linke and Goldsmith (1980) and Liszt and Leung (1977). We have analyzed our results using these models. The calculated values for $n(H_2)$ from both models in fact agree quite well, so that the particular model of radiation transfer appears unimportant. This was attributed by Linke and Goldsmith (1980) to the modest opacities of the CS lines. An important aspect of the analysis of CS data is the careful accounting of the effects of different beam sizes employed to study the different transitions. As pointed out by both Liszt and Leung (1977) and Linke and Goldsmith (1980), even after absolute calibration has been accomplished, the fact that CS emission regions are small results in unequal beam dilution effects. For example Linke and Goldsmith observed the 2–1 line with the 2.'1 beam of the Bell Telephone Laboratories antenna and the 1–0 line with the 2.'6 beam (somewhat smaller than what we measured) of the NRAO 36 foot (11 m) telescope. They estimate that a possible relative dilution effect of $\lesssim 23\%$ may still be present in their data. With our even more discrepant beam sizes of 1.'5 and 2.'7, we sought to account for

this effect by mapping the region to obtain a good estimate of the size, and then explicitly removing the effects of the beam filling factor Φ.

For NGC 7538 (Figs. 2*a*, *b*), we can estimate the FWHM of the emission regions to be $\sim 6'.0 \times 4'.0$ ($\alpha \times \delta$) for the $J=1-0$ line and $\sim 3'.0 \times 3'.5$ for the $J=2-1$ line. The large size of the $J=1-0$ emission region relative to the $J=2-1$ region is due in part to beam broadening. However after removal of this effect, the $J=1-0$ region is still $5'.4 \times 3'.0$ while the $J=2-1$ region is $2'.6 \times 3'.2$. This apparent larger spatial extent in right ascension for the $J=1-0$ line may be due to an optical depth effect. We have made observations in the ^{34}S isotope of CS which can be used to deduce the optical depth in the ^{32}S isotope:

$$\tau_{32} = 22.5\,\tau_{34} = -22.5 \ln\left\{1 - \frac{\Delta T^*_{a34}}{\Delta T^*_{a32}}\left[\frac{\Phi_{32}}{\Phi_{34}}\frac{J_\nu(T_{ex32}) - J_\nu(T_b)}{J_\nu(T_{ex34}) - J_\nu(T_b)}\right]\left[1 - \exp(-\tau_{32})\right]\right\}, \tag{10a}$$

where subscripts denote the particular isotope, and the isotopic ratio $[^{32}S]/[^{34}S]$ is taken to be the terrestrial value of 22.5. Since $\Phi_{32} > \Phi_{34}$ because the $C^{32}S$ line will be more optically thick, and $T_{ex32} > T_{ex34}$ because of radiative trapping effects, we can set the lower limits:

$$\tau_{32} \geq -22.5 \ln\left\{1 - \frac{\Delta T^*_{a34}}{\Delta T^*_{a32}}\left[1 - \exp(-\tau_{32})\right]\right\}. \tag{10b}$$

We observe the ratio $\Delta T^*_{a34}(2-1)/\Delta T^*_{a32}(2-1) = 0.22 \pm 0.05$ and $\Delta T^*_{a34}(1-0)/\Delta T^*_{a32}(1-0) < 0.07$. This corresponds to $\tau_{32}(2-1) \geq 5.7 \pm 1.4$ and $\tau_{32}(1-0) < 0.9$ when equation (10b) is solved. We note that $\tau_{32}(1-0)$ is not given as a lower limit because we expect trapping enhancement of T_{ex32} and optical depth effects on Φ_{32} to be unimportant in this case because of the probable low opacity for this line. Hence the $J=1-0$ line is optically thin while the $J=2-1$ line is optically thick. The different size scales of the emission regions in these CS lines may therefore be the natural consequence of the fact that the $J=1-0$ line, being thin, will sample the column density distribution while the $J=2-1$ line, being thick, will sample the excitation temperature distribution. The implications of these conclusions are more fully discussed in the next section.

Returning to the question of density, we now remove unequal beam dilution effects by considering two alternatives: first, we can try convolving the $J=1-0$ map with a $2'.7$ beam; second, we can remove beam dilution effects from both maps by assuming the source size to be that measured in the $J=2-1$ line. Referring to the discussion above, we see that there will be some contamination from low excitation gas in the $J=1-0$ line. Hence deduced densities may be lower limits. Using the former approach we find $R(2/1) = \Delta T^*_a(2-1)/\Delta T^*_a(1-0) = 0.91^{+0.06}_{-0.04}$ with $\Delta T^*_a(2-1) = 2.9 \pm 0.05$ K. Using the later approach, we find the same value for the ratio $R(2/1)$ as we must with $\Delta T^*_a(2-1) = 5.3 \pm 0.1$ K. Referring to the calculations of Linke and Goldsmith (1980) and assuming $T_k \sim 30$ K, we find $n(H_2) \sim 3 \times 10^4$ cm^{-3} for NGC 7538 from CS measurements. This is in good agreement with their results if we correct their value of 6×10^4 cm^{-3} downward to account for the additional beam dilution effect suffered by the $J=1-0$ line.

The other source toward which we have CS data is W33 B. However, because of the low intensity of this source, mapping results were inconclusive. Formally $R(2/1) = 1.7^{+0.6}_{-0.4}$ for the center position. Assuming $T_k \sim 20$ K, calculations of Linke and Goldsmith (1980) indicate $n(H_2) \sim 2 \times 10^5$ cm^{-3}. However, unequal beam dilution effects as discussed above may lower this estimate. For example, if the emission region is $\sim 1'$ as for NH_3, we find $R(2/1) \sim 0.7 \pm 0.2$ with $\Delta T^*_a(2-1) \sim 2.3$ K. This would imply a density $n(H_2) \sim 2 \times 10^4$ cm^{-3} with uncertainties approaching factors of a few.

We note that the multilevel non-LTE statistical equilibrium calculations of Linke and Goldsmith (1980) and Liszt and Leung (1977) may not be entirely realistic treatments of CS excitation due to (1) assumption of uniform density, (2) spherical geometry, and (3) the fact that calculated opacities may be lower than the observed values. The value of the calculated opacity can be adjusted through the abundance or velocity gradient parameter adopted in their calculations. However, the increased opacity may affect the details of the numerical results.

III. DISCUSSION

Here we will discuss in detail the results of our analysis. We are interested in the general physical characteristics of the clouds which we have found associated with the compact and the ultracompact H II regions. The possible dynamical relationship between the neutral cloud and the H II regions, the heating and cooling processes within the clouds, and different star formation schemes will also be examined.

a) *Clumping*

Whether the NH_3 emission in fact fills the beam at Haystack and Effelsberg is an important question not only with regard to obtaining more accurate estimates of size scales, densities, and masses, but also with regard to the question of clumping in NH_3 and possibly other molecules (cf. Ho *et al.* 1979; Evans, Plambeck, and Davis 1979). By clumping we mean density variations on a scale small compared to the antenna beam. It is clear that the effects of clumping may not be observable in all spectral lines that are studied. This is due to the optical depth effects. If the line is heavily saturated as for CO, we expect radiative trapping effects to thermalize the transition even in between clumps where the density is low. If the line is optically thin, then all we measure is the total column density within the beams. In both these cases the actual physical distribution of the molecules, i.e., in clumps or not, will not affect the observational results. However, in the regime where opacities are moderate with $\tau \sim 1$ so that trapping effects are not severe, and where the transition is not thermalized in between clumps so that effects of density contrasts are important, clumping will have observable consequences. In particular, in comparing different molecular species or even different transitions of the same molecule, we must consider the effects of different beam sizes and different optical depths.

One method of studying this problem is to vary the antenna beamwidth used to study the same molecular transition. In the case of Orion, a comparison of observations at Haystack (Barrett, Ho, and Myers 1977) and Effelsberg (Wilson, Downes and Bieging 1979) confirmed the existence of a small clump of NH_3 emission probably associated with the cluster of infrared objects in the vicinity of the Kleinman-Low nebula (Rieke, Low, and Kleinmann 1973; Wynn-Williams and Becklin 1974). We used this technique (see § II*c* above). From Figure 4, we conclude that in fact size scales of the NH_3 emission regions are typically $\lesssim 1'$ so that they are at least comparable to the Effelsberg beam. Table 7 summarizes the deduced results for the six sources in terms of size scales. The error bars reflect the 1 σ uncertainties in ΔT_a^*, and the uncertainties in the geometry of the emission regions. We also compute the expected values of Φ and hence T_{ex} and $n(H_2)$ at both telescopes. A modest amount of clumping with a filling factor of 30–50% is found with respect to the Haystack beam. We also compare this size scale, from a comparison of observations with different beam widths, with the FWHM extent of the emission from mapping, after corrections for beam broadening. The value of $\theta_s/2R'$ is ~ 0.3–0.5. We therefore conclude that the NH_3 emission regions that we have mapped are typically composed of several smaller pieces whose size scale is on the order of 1 pc.

The above analysis considered the case for a single clump. We also consider the case where numerous clumps with a scale of 0.01–0.1 pc exist. We calculate the contributions of many clumps from equation (1) by substituting for the filling factor $\Phi = n_c\theta_s^2/\theta_b^2$, where n_c is the number of clumps and θ_s/θ_b is the ratio of clump size to beam size. Assuming optically thick clumps, we estimate at a distance D

$$\Delta T_a^* \approx 2.42 \left[\frac{T_{ex}}{10\ \mathrm{K}}\right]\left[\frac{n_c}{10}\right]\left[\frac{\theta_s}{0.1\ \mathrm{pc}}\right]^2\left[\frac{D}{3\ \mathrm{kpc}}\right]^{-2}\left[\frac{\theta_b}{43''}\right]^{-2} \mathrm{K}. \quad (11)$$

If n_c is large and if the distribution of clumps is uniform, equal values of ΔT_a^* would be obtained at both telescopes. The maximum contribution from *many* unresolved clumps, essentially a "background" emission, would then be limited by the values of ΔT_a^* from Haystack which were typically ~ 1 K. Assuming $n_c = 10$, the observations are consistent

TABLE 7

DERIVED DENSITIES AND SIZE SCALES FROM COMPARISON OF HAYSTACK AND EFFELSBERG DATA

Source	θ_s (″)	$\Phi(43'')$	T_{ex}[a] (K)	$n(H_2)$ (cm^{-3})	$\Phi(84'')$	T_{ex} (K)	$n(H_2)$ (cm^{-3})
OH 10.6	25^{+29}_{-25}	$0.25^{+0.36}_{-0.25}$	$46\ ^{+\infty}_{-25}$	$>7.0\times10^4$	$0.08^{+0.21}_{-0.08}$	$32^{+\infty}_{-21}$	$1.3^{+\infty}_{-1.3}\times10^6$
W33 B	62^{+31}_{-26}	$0.68^{+0.15}_{-0.26}$	$7.7^{+3.0}_{-0.9}$	$1.0^{+1.1}_{-0.2}\times10^4$	$0.35^{+0.20}_{-0.20}$	$6.9^{+5.5}_{-1.5}$	$9.3^{+2.8}_{-4.0}\times10^3$
W33 A	52^{+24}_{-22}	$0.59^{+0.16}_{-0.27}$	$15\ ^{+10}_{-3}$	$5.8^{+\infty}_{-2.8}\times10^4$	$0.28^{+0.17}_{-0.16}$	$13\ ^{+13}_{-3.9}$	$3.3^{+\infty}_{-1.8}\times10^4$
OH 69.5	70^{+23}_{-23}	$0.73^{+0.10}_{-0.18}$	$7.0^{+1.4}_{-0.5}$	$8.9^{+4.3}_{-1.3}\times10^3$	$0.41^{+0.14}_{-0.17}$	$7.2^{+3.0}_{-1.2}$	$7.9^{+8.0}_{-2.5}\times10^3$
W75 N	85^{+41}_{-33}	$0.80^{+0.10}_{-0.20}$	12^{+3}_{-1}	$1.6^{+0.8}_{-0.2}\times10^4$	$0.51^{+0.19}_{-0.23}$	$6.1^{+2.7}_{-0.9}$	$5.4^{+5.8}_{-1.6}\times10^3$
NGC 7538 .... (0, −80″)	69^{+24}_{-23}	$0.72^{+0.10}_{-0.19}$	$8.5^{+2.1}_{-0.7}$	$1.3^{+0.8}_{-0.3}\times10^4$	$0.40^{+0.15}_{-0.17}$	$8.8^{+4.5}_{-1.6}$	$1.1^{+1.5}_{-0.4}\times10^4$

[a] T_{ex} and $n(H_2)$ are derived from data with 43″ and 84″ resolution, assuming source size to be θ_s. Derived quantities are then in good agreement between the two telescopes.

with clump sizes $\sim$0.06 pc, similar to values in Orion (Ho *et al.* 1979). We note that a clumped but unresolved background is indistinguishable from a smooth one based on the present arguments. The excess emission observed at Effelsberg ($\sim$1$-$4 K; see Fig. 3) must still be explained as before, where the emission is dominated by a single clump (see Fig. 4). However, the removal of a background lowers the estimates of the size scale. From equation (11) we see that a single clump with a size $\gtrsim$0.1 pc can explain the excess emission observed at Effelsberg for reasonably high values of $T_{ex} \sim 50$ K. The size scale cannot be much smaller unless T_{ex} is very high.

We therefore conclude our discussion on clumping in these regions as follows: (1) The observations can be explained by emission regions with sizes on the order of 3 pc, which are composed of several smaller fragments on the order of 1 pc. These smaller fragments are beginning to be resolved by the Effelsberg antenna. (2) Clumping on a smaller scale with many unresolved clumps within the beam may also be present. However, the low values of ΔT_a^* at Haystack constrain the clump size to be $\lesssim 0.06$ pc $[n_c/10]^{-1/2}[T_{ex}/50\ \mathrm{K}]^{-1/2}$, where n_c is the number of clumps within the Effelsberg beam. (3) The excess emission at Effelsberg can then also be explained by the presence of a central core with a high temperature and a size ~ 0.1 pc $[T_{ex}/50\ \mathrm{K}]^{-1/2}$.

Whether clumping on the scale of 0.1 pc exists in these regions must be determined from density arguments. If case 1 above is true, deduced values of $n(H_2)$ are as in Table 7, on the order of 10^4 cm^{-3}. If case 2 is true, deduced values for $n(H_2)$ will be very high, $n(H_2) \gtrsim 10^5$ cm^{-3}. Arguments based on estimates of masses may also be useful in discriminating between these models.

b) Densities

It is clear that the determination of densities in interstellar clouds is an important question. Numerous molecules have been used systematically in attempting to deduce values of $n(H_2)$ including H_2CO (Wooten *et al.* 1978), CO (Plambeck and Williams 1979), CS (Linke and Goldsmith 1980), SO (Gottlieb *et al.* 1978), CH_3OH (Gottlieb *et al.* 1979), and HC_3N (Vanden Bout *et al.* 1981). Whereas $n(H_2)$ deduced from the latter four molecules are in general good agreement, H_2CO consistently yield higher estimates while CO consistently yield lower estimates. The problems in reaching a consensus are numerous, and some may be fatal: (1) In general, multilevel analysis is necessary because of the large number of energy states involved. This is especially true for the asymmetric rotors. This means that collision cross sections between various states must be determined, which is usually a difficult experimental exercise. In general one must rely on ab initio calculations. (2) Optical depths may be high, in which case radiative trapping effects must be accounted for. (3) Because of large differences in the frequencies of the transitions, the antennas usually have very different beamwidths. (4) Because of excitation conditions, different molecules and even transitions within the same molecule are usually not spatially coextensive. Hence the derivation of densities from a single molecular species and the comparisons between different molecules are usually ungratifying experiences.

The metastable NH_3 transitions which we study here have the advantage of being well isolated in the sense that transitions across K-ladders tend to be slow while decays from the upper nonmetastable states in each K-ladder are fast. The excitation problem is therefore amenable to analysis using a two-level model. Statistical equilibrium calculations by Morris *et al.* (1973) indicate this approximation to be fairly accurate for $T_k < 100$ K and $n(H_2) \lesssim 10^5$ cm^{-3}. The greatest uncertainty is actually due to the adopted values of the collision cross sections. In our calculations and that of Morris *et al.* (1973), a hard-sphere collision cross section of 2.5×10^{-15} cm^2 is assumed for the (1,1) transition (Oka 1968). Schwartz (1979) suggests from extrapolation of laboratory line width data at room temperature that the cross section at $T_k = 20$ K is a factor of 6 greater if the collisions between NH_3 and H_2 are dipole-quadrupole in nature. Green (1980) on the other hand calculates an equivalent NH_3–He cross section at $T_k = 20$ K which is 0.63 times the value we used. Correcting up for NH_3–H_2 collisions where the H_2 molecules may be in the ortho state, these cross sections are in good agreement with our adopted values. We think the cross sections are not likely to be as large as Schwartz calculates for the following reasons: (1) The required density to thermalize the NH_3 transition becomes very low: $T_{ex}(1,1) = 0.9T_k$ for $n(H_2) \lesssim 10^4$ cm^{-3}, $T_{ex}(1,1) = 0.5T_k$ for $n(H_2) \lesssim 10^3$ cm^{-3}. Ammonia should therefore be easily excited over extended regions in interstellar clouds on a scale comparable to CO. (2) Observed NH_3 opacities are usually substantial with $\tau \sim 1$ from hyperfine analysis so that, unless abundance gradients are sharp, the NH_3 emission should be observable over large extended regions. (3) In fact, NH_3 emission is well localized, with spatial extents comparable to other molecules requiring high densities for excitation such as CS (see Figs. 1*i* and 2*b*) or HC_5N (Myers, Ho, and Benson 1979). This is especially true in dark clouds where spatial extents of different molecules have been measured (Martin and Barrett 1978). (4) In dark clouds, NH_3 line widths are typically very narrow (Ho *et al.* 1977) compared to other molecules. This again implies that the emission are spatially confined. Thus if NH_3 cross sections are large, the low density and small spatial extent of its emission in dark clouds must be reconciled with higher density estimates from other molecules. If one resorts to clumping arguments for these nearby clouds, one finds the necessity of postulating small-scale structures on the order of 0.01 pc. Furthermore, density contrasts on such small scales must be large because of the low densities required to excite NH_3 under the assumption of a large collision cross section.

We have argued for the reliability of the adopted cross section. We estimate that the densities deduced from NH_3 observations are probably reliable to a factor of 2. In § II*c*, we discussed the results of CS observations which were intended for an independent estimate of the densities. We find that the comparison of the two CS transitions at two very different frequencies involved a myriad of problems such as absolute and relative calibration (see § II*a*), unequal beam dilution effects, noncoextensive emission regions, and unequal optical depth effects. In particular, our $C^{34}S$ observations indicate that $\tau_{32}(2-1)$ may be large, which may complicate the radiative transfer analysis reported by Liszt and Leung (1977) and Linke and Goldsmith (1980). However, after corrections for most of these effects, we find that the NH_3 (Table 7) and CS (§ II*c*) results agree within the errors in the deduced value of $n(H_2)$ for NGC 7538. This is consistent with the good agreement in the shapes of the NH_3 map and the CS $J=2-1$ map, which may be due to the fact that both lines have similar opacities.

This agreement between CS and NH_3 in the determination of $n(H_2)$ appears to favor the less severe clumping model discussed in § III*a* where the small scale structure is on the order of 1 pc. However, we note that a more severe clumping model with many clumps still cannot be ruled out. The reason is that the CS $J=2-1$ line, being moderately optically thick, will be more affected by clumping. Hence if corrected for clumping, the ratio $R(2/1)$ for the two CS lines would be higher, implying higher densities. Clumping on the scale of 0.1 pc would then be consistent with both CS and NH_3 observations. Mass estimates also do not argue against this model of multiple small-scale structures. Table 6 lists masses for the $\Phi=0.1$ case. The calculated mass is that of a single clump, $\sim 2\times 10^4\ M_\odot$ in the case of NGC 7538. For n_c clumps within the beam, mass per clump can be derived by multiplying approximately by $n_c^{-3/2}$. From equation (3), we see that

$$\frac{M/n_c}{M_\odot} = 3.9\times 10^3 \left[\frac{D}{1\ \mathrm{kpc}}\right]^3 \left[\frac{n(H_2)}{10^5\ \mathrm{cm}^{-3}}\right] \left[\frac{\theta_b}{1'.5}\right]^3 \left[\frac{\Phi/n_c}{1-\Phi/n_c}\right]^{3/2}; \tag{12a}$$

$$\frac{M}{M_\odot} = 1.2\times 10^2 \left[\frac{D}{1\ \mathrm{kpc}}\right]^3 \left[\frac{n(H_2)}{10^5\ \mathrm{cm}^{-3}}\right] \left[\frac{\theta_b}{1'.5}\right]^3 \left[\frac{\Phi}{0.1}\right]^{3/2} n_c^{-1/2}. \tag{12b}$$

Both total mass and mass per clump can be lowered by allowing for an appropriately large value for n_c. The proposed picture of many clumps of $\lesssim 100\ M_\odot$, each confined to ~ 0.1 pc, therefore appears possible. The possibility of the presence of a single clump with high density and high temperature also cannot be eliminated using these arguments. It may in fact be supported by the mapping data at Haystack and Effelsberg where the telescopes were pointed off the emission peaks. Equal intensities at both telescopes in these cases (see Fig. 3) may suggest a background emission which in turn suggests that the emission peaks are due to an unresolved source. We must keep in mind, though, that sidelobe responses may be important for the spectra off the peak.

We have attempted to resolve the question of clumping by deducing densities from CS measurements. Despite an apparent agreement between CS and NH_3, we still cannot rule out possible clumping effects on the $J=2-1$ line of CS. Mass estimates for the cases both with and without clumping also did not set sufficiently stringent limits that would allow the discrimination against either model. Until better estimates of $n(H_2)$ can be made, or until interferometric measurements actually set the limits on clump sizes, both models proposed above for the molecular clouds associated with the UCHII regions remain viable.

c) General Cloud Properties

There are several general conclusions which we can draw about the properties of the molecular clouds associated with the UCHII regions.

1. These are warm clouds with a range $14<T_R<29$ K corresponding to the values $20<T_k<41$ K. These temperatures are intermediate between cool dark clouds with $T_k\sim 10$ K (Dickman 1975; Martin and Barrett 1978), and the more massive molecular clouds with $T_k\gtrsim 50$ K associated with sources of high luminosity (e.g., Orion, M17). As discussed in § II*c*, from the agreement on T_k as deduced from observations at Haystack and Effelsberg, we find that any embedded source with significantly higher values of T_k must be smaller than 25″ (0.36 pc at a distance of 3 kpc) in size. This is consistent with a core-halo type model discussed above which explains the enhanced value of ΔT_a^* observed at Effelsberg. At the same time coarse sampling of the CO distribution indicates that observed values of T_k for some of the sources are local maxima on the scale of 3′ while for the other sources T_k may be enhanced over regions $\gtrsim 6'$ in size.

2. If T_k is constant, the observed NH_3 peaks are likely to correspond to local density maxima. Alternatively a local maximum in T_k is also possible as in the case of OH 10.6. Nevertheless the decrease in NH_3 intensity away from the UCHII regions is in general much sharper than the decrease in CO intensity. Hence the NH_3 peaks are probable

density maxima or at least column density maxima. We favor the former possibility, as mapping results in regions such as NGC 7538 (see Table 3C) indicate an actual peak in T_{ex} but not in T_R. As discussed in the case of Orion (Ho *et al.* 1979), peaks in NH_3 emission can also be due to variations in the beam filling factor. For a clumpy cloud, this effect may also be important.

3. Adopting the definitions of Israel, Habing, and de Jong (1973), we find that eight out of the 10 clouds which we studied contain UCHII regions while four of them contain CHII regions. We have plotted the positions of the continuum sources on the maps of the NH_3 emission (see Figs. 1*a*–1*j*). We find that, with the exception of S140, all of the UCHII regions lie essentially within the 80% contours of the NH_3 emission peaks; S140 is at the 50% contour. All of the CHII regions also lie within the 50% contour of the NH_3 peaks, with W75 N and S156 A farther in, and S235 AB and S255 apparently farther out. In this regard it is useful to note that the deduced electron densities for the CHII regions in S235 AB and S255 are a factor of 3 lower than their corresponding values in W75 N and S156 A, which in turn are lower by factors $\gtrsim 3$ than the densities in UCHII regions. The smaller and denser H II regions therefore appear more centered with their NH_3 distribution. However, we must caution that in fact the NH_3 emission regions are not fully resolved in many cases because of the large distances to them. Whether the H II regions are well correlated with the neutral cloud is therefore uncertain. Note especially in the case of S140, although the UCHII region appears to be at the half-power point of the NH_3 emission, the actual projected spatial separation is comparable to the other regions simply because it is a factor of 3 closer to us. That the CHII regions appear to be displaced farther from the NH_3 peaks than are UCHII regions may also be due in part to this effect.

4. Size scale of the NH_3 emission regions and other characteristics of the emission are similar to those observed in the Orion region. If the Orion molecular ridge were at a distance of 3 kpc, the NH_3 emission would be extended on a scale of 2.5, similar to values in Table 6. Gull and Martin (1975) using aperture synthesis techniques constructed a high resolution (7″×20″) map of Orion at 5 GHz. They find structures smaller than 0.1 pc, similar to the regions studied here. Observed NH_3 line widths, deduced densities, and masses are also similar, although deduced temperatures are somewhat higher for Orion. Depending on the actual value for the densities in these clouds, clumping in the NH_3 emission associated with the UCHII regions may also be present. The appealing possibility may be advanced: the UCHII regions may be the less evolved versions of an Orion-type region, with an H II region embedded in a large cloud, located at large distances.

5. Observed line widths are large. Typical values of a few km s^{-1} are similar to the values for more turbulent(?) clouds associated with H II regions. However, no single type of dynamical process—e.g., radial motion—is apparently dominant in all instances. In the case of NGC 7538 (Table 3C), an apparently well localized enhancement in line width is observed, consistent with radial collapse or expansion. On the other hand, significant velocity gradients may be present toward some of the regions. Hence beam averaging over Doppler shifted emission may account for substantial portions of the line widths. At a typical distance of 3 kpc, a velocity gradient of 1 km s^{-1} pc^{-1} would imply a velocity dispersion of ~ 1 km s^{-1} over our beam. Line blending between two nearby velocity components may also be important as in the case of W33 A. It is also uncertain whether clumping will have a dominant effect on line width, although different line widths observed at different telescopes may be explained in this manner. Specific cases will be discussed in a later paper.

6. Despite the uncertainty in the importance of clumping, and the consequent uncertainty in densities, deduced total masses for these regions are fairly well determined. Table 6 summarizes the calculated masses for the unclumped ($\Phi=1$) case and the single clump ($\Phi=0.1$) case. The total mass for the multiple clumping case can be obtained by lowering the single clump masses by $n_c^{-1/2}$ (see eq. [12]). That the total mass is a slow function of clumping is due to the fact that the deduced densities rise sharply with decreasing size scales, sufficiently to compensate for the decreasing volume. We therefore find typical masses in the range 10^2–10^4 $M_\odot$. The lower end of the deduced masses (see Table 6) clearly belongs to the group of clouds associated with CHII regions. With the exception of S140, the masses of the clouds associated with UCHII regions tend to be in the range 10^3–10^4 $M_\odot$. We also find that deduced masses in general exceed the critical masses for gravitational stability. This conclusion appears to be independent of clumping, since M_c will decrease as $n(H_2)$ increases. The only cases where deduced masses are comparable to the calculated values of M_c are the two clouds associated only with CHII regions and S140.

7. Deduced cloud densities and size scales from NH_3 observations can be compared to the CO observations in order to estimate the relative contributions of the NH_3 clouds to the total column densities along the line of sight. We first estimate the column density $N(H_2)$ from the NH_3 data in Table 6 directly as $N(H_2)_{NH_3}=2R'n(H_2)$. We then estimate $N(H_2)$ from the CO data by assuming a value for the abundance ratio $\xi=N(CO)/N(H_2)$. After correcting for the different beam sizes, we arrive at the expression

$$f=\frac{N(H_2)_{NH_3}}{N(H_2)_{CO}}=\frac{2R'n(H_2)\xi}{N(CO)}\left[\frac{(2R')^2}{(2R')^2+\theta_b^2(CO)}\right], \tag{13}$$

where θ_b(CO) is the CO beamwidth. Adopting Dickman's (1978) value of $\xi^{-1}=5.6\times10^3$ appropriate for the terrestrial isotopic ratio [CO]/[^{13}CO]=89, we find an average value for our sample $\langle f\rangle=0.62\pm0.41$ for the case $\Phi=1$ and a value $\langle f\rangle=1.06\pm1.84$ for the case $\Phi=0.1$ and $n_c=1$. This implies that the dense clouds which we have found to be associated with UCHII regions can constitute a major portion of the total column density along with line of sight. This conclusion is directly dependent on the value of ξ. Wootten *et al.* (1978) have argued for a lower value for ξ by an order of magnitude in regions of moderate temperatures ($T_k>20$ K) and high densities [$n(H_2)>10^5$ cm^{-3}]. However, almost certainly the bulk of the CO emission in fact arises from regions of lower temperature and lower density. Hence Dickman's value for ξ is probably the best value to use in equation (13). We note that just as in the calculation of M in equation (12), the value of f will be lowered by $n_c^{-1/2}$ for the multiple clumping case. For sufficiently large number of clumps, the bulk of the cloud matter along the line of sight will then reside outside of the clumps.

d) OB Star Formation

One of the main objectives of studying CHII and UCHII regions in the molecular lines is to estimate the mass M of the associated molecular clouds. Such estimates are meaningful in these cases because the H II regions are still small so that ambient clouds in all likelihood have not yet been disrupted. Reliable values for M can then be used to assess the efficiency of star formation.

We are interested in whether a correlation exists between the mass of a cloud and the maximum stellar mass that can be formed. We estimate the mass M_* for the largest star in each region from the radio data (see references in Table 2), although these are likely to be lower limits if the Lyman continuum photons are absorbed by dust within the H II regions. Far-infrared measurements, on the other hand, do provide a better estimate for the total energy output of a star, thereby setting upper limits on M_*.

We compare M with M_* in Figure 7. Values of M are plotted as error bars indicating the uncertainty in clumping. Values of M_* are as deduced from the radio data. Wherever far-infrared data are also available, upper limits to M_* are indicated by the dashed arrows.

We find a rough correlation between M and M_*. With the far-infrared measurements of S140, S255, and S235 AB (Harvey, Campbell, and Hoffman 1978; Beichman, Becklin, and Wynn-Williams 1979; Evans *et al.* 1981), it is clear

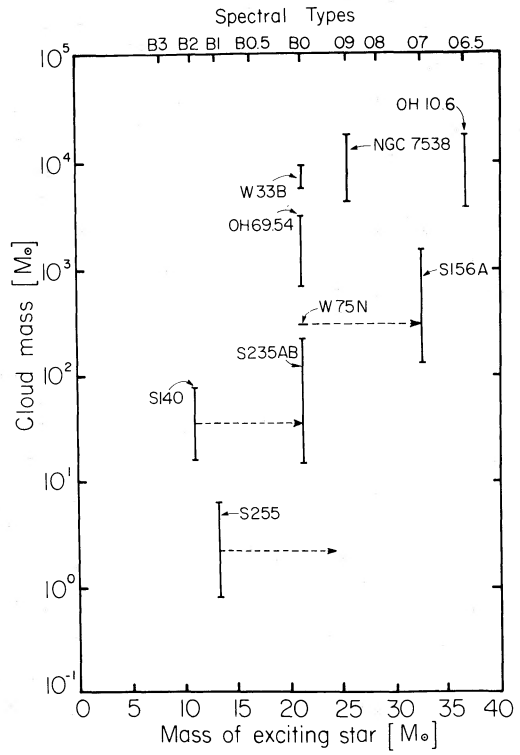

FIG. 7.—A comparison of stellar mass M_* for the largest star in each region with the associated cloud mass M. Dashed arrows indicate upper limits on M_* as deduced from far infrared data. In the case of S235 AB, the far-infrared data are consistent with the B0 star. Error bars for M correspond to uncertainties in the filling factor Φ. For multiple clumps, M can be lowered by $n_c^{-1/2}$.

that these clouds do not contain stars with spectral types much earlier than B0. At the same time it is clear that for those regions with O stars such as OH 10.6 and NGC 7538, $M > 10^3\ M_\odot$. Together these data suggest that O stars are not likely to be found in cloud fragments with $M \lesssim 10^2\ M_\odot$.

The observed value of M_*/M for the largest star in each region can be compared with theoretical calculations. In particular Larson (1978) has carried out calculations of the three-dimensional collapse and fragmentation of isothermal clouds. One major finding is that the maximum mass that can be accreted by a single object is a function of the angular momentum and the viscosity of the gas. For a Reynolds number $\Re \approx 50$, Larson finds that the initial ratio of rotational energy to gravitational energy β must be less than $\sim 20\%$ if more than 20% of the initial cloud mass is to be accreted. For a Gaussian density distribution, the gravitational energy is $(\ln 2/\pi)^{1/2} GM^2/R$, the rotational energy for rigid-body rotation is $(2\ln 2)^{-1} MR^2 (dV/dR)^2$, where $M = (\pi/\ln 2)^{3/2} m_{H_2} n(H_2) R^3$ is the mass, R is the cloud radius, $m_{H_2} n(H_2)$ is the peak mass density, and dV/dR is the velocity gradient. We can therefore write

$$\beta = 0.107 \left[\frac{n(H_2)}{10^4\ \mathrm{cm}^{-3}} \right]^{-1} \left[\frac{dV/dR}{1\ \mathrm{km\ s}^{-1}\ \mathrm{pc}^{-1}} \right]^2 . \tag{14}$$

Hence our observation that $M_*/M \gtrsim 20\%$ for stars later than B0 in our sample suggests that if star formation occurred via collapse as described by Larson (1978), the initial density must have been

$$n(H_2) \gtrsim 5 \times 10^3\ \mathrm{cm}^{-3} \left[\frac{dV/dR}{1\ \mathrm{km\ s}^{-1}\ \mathrm{pc}^{-1}} \right]^2 . \tag{15}$$

This value for $n(H_2)$ can be lowered by a factor of ~ 2 if the density distribution were uniform. Thus unless the angular momentum of the cloud has been dissipated early on so that $dV/dR < 1$ km s^{-1} pc^{-1}, we draw the further conclusion that $n(H_2)$ must be substantial at the initiation of collapse and fragmentation. This result is apparently insensitive to cloud temperature (Larson 1978).

That the O stars are associated only with the more massive clouds with $M > 10^3\ M_\odot$ suggests that collapse and fragmentation processes (e.g., Larson 1978; Bodenheimer 1978) may not be dominant in these cases. Certainly processes such as radiation pressure and stellar winds are more important for the O stars in reversing the normal accretion process, thereby limiting M_*. A more radical and more efficient means of accretion would then be needed as proposed by McCrea (1960), Silk (1978), Silk and Takahashi (1979), and Larson (1980). In these models, formation of high-mass stars are aided by the accumulation and coalescence of smaller clumps. The presence of supersonic motion in these molecular clouds, argued by Larson (1980) to be turbulence, and the possibility of a clumpy cloud structure (§ III*a*, *b*) suggest that indeed clump-clump interaction may be important. In this scenario, isolated lower mass cloud fragments will not be able to build massive stars.

We conclude that for our limited sample of UCHII and CHII regions, we find a correlation between the mass of the largest star in the region and the mass of the associated cloud fragment. For stars later than B0, their formation may be consistent with the collapse and fragmentation model of Larson (1978). For the more massive O stars which were *not* found in the less massive regions, we argue that fragment collisions and subsequent coagulations may be important processes which must be considered.

e) Thermal Balance

We consider the role of compact H II regions in the balance of heating and cooling within molecular clouds. We will treat the dust and the gas separately. This is justified since the dust cooling rate is so large that thermal balance for the dust is established independent of the gas. For sufficiently high densities, some of the radiant energy absorbed by the dust can be transferred to the gas via collisions. Dust grains therefore serve as an intermediary to couple the gas to an embedded source. Whether the compact H II regions are significant sources of heat for the gas can now be examined by a comparison of the various heating and cooling processes.

We first consider the dust energetics. Assuming a blackbody spectrum, the cooling rate for the dust can be obtained by integrating over frequency and space,

$$\Lambda_d = \int_{r_*}^{R} dr\, 4\pi r^2 n_d(r)\, 4\pi s^2 \int_0^\infty d\nu\, \pi B_\nu [T_d(r)]\, a(\lambda), \tag{16}$$

where n_d is the dust density, s is the grain radius, r_* and R are respectively the radius of the star and the cloud, B_ν is the Planck function, T_d is the dust temperature, and $a(\lambda)$ is the dust emissivity which is also the absorptivity. We have

assumed that spherical symmetry applies and that the grain emission will be optically thin. We further recognize that the dust optical depth can be related to $a(\lambda)$ (Goldreich and Kwan 1974):

$$\tau_d(\lambda)=\int dr\, n_d(r)\pi s^2 a(\lambda). \tag{17}$$

By parametrizing $a(\lambda)=a_0\lambda^{-\alpha}$, the frequency integral in equation (16) can be performed directly. Specializing to the uniform density and isothermal case, we can normalize a_0 by the observed value of τ_d, thereby obtaining, for $0<\alpha<2$ and $R\gg r_*$,

$$\Lambda_d\sim 1\times 10^4 L_\odot\left[\frac{T_d}{30\,\mathrm{K}}\right]^{4+\alpha}\left[\frac{2R}{1\,\mathrm{pc}}\right]^2\left[\frac{\tau_d(100\,\mu\mathrm{m})}{0.05}\right]. \tag{18}$$

The adopted value of τ_d can be shown to be reasonable. For $T_d>30$ K, the bulk of the dust emission will be in the far-infrared. Both Righini-Cohen and Simon (1977) and Evans, Blair, and Beckwith (1977) have argued that the far-infrared optical depth can be related to the ^{13}CO column density. Adopting the relation $\tau_d(100\,\mu\mathrm{m})=10^{-18}N(^{13}\mathrm{CO})$ and the values of $N(^{13}\mathrm{CO})$ from Table 5, we find a typical value $\tau_d\sim 0.05$. Equation (18) can be interpreted to mean that a main sequence star of spectral type earlier than B0.5 (Panagia 1973) will be required to support the far-infrared emission of a cloud with a diameter of 1 pc at an average dust temperature of 30 K. Of course, temperature and density will not be uniform in a real cloud with an embedded source. In particular the intensity of star light falls off with r^{-2}, the square of the distance to the star. To determine an upper bound on T_d as a function of r, we balance the cooling rate of a single grain against its heating rate. The maximum heating rate can be obtained by assuming unattenuated star light and complete dust absorption, i.e., $a(\lambda)=1$ for the bulk of the stellar emission (Goldreich and Kwan 1974). We obtain for a stellar temperature T_*,

$$4\pi s^2\int_0^\infty d\nu\,\pi B_\nu[T_d(r)]a(\lambda)\approx\pi s^2\int_0^\infty d\nu\,\pi B_\nu[T_*]\,r_*^2/r^2. \tag{19}$$

Expressing the solution in observable quantities, we find for $0<\alpha<2$:

$$T_d(r)\sim 50\,\mathrm{K}\left[\frac{5\times 10^{16}\,\mathrm{cm}^{-2}}{N(^{13}\mathrm{CO})}\frac{\langle n(\mathrm{H}_2)\rangle}{10^4\,\mathrm{cm}^{-3}}\frac{2R}{1\,\mathrm{pc}}\frac{s^2}{(6\times 10^{-6}\,\mathrm{cm})^2}\right]^{1/4+\alpha}\left[\frac{L_*}{10^4 L_\odot}\right]^{1/4+\alpha}\left[\frac{2r}{1\,\mathrm{pc}}\right]^{-2/4+\alpha}, \tag{20}$$

where L_* is the stellar luminosity. The dependence on $N(^{13}\mathrm{CO})$, $n(\mathrm{H}_2)$, R, and s are explicitly shown to demonstrate that dust properties must either be assumed or inferred from observations. Equation (20) in fact is a fairly good estimate of T_d despite the omission of dust extinction and heating from dust reradiation; this is due to the fact that the latter process will compensate for the former (Scoville and Kwan 1976). A comparison of equations (18) and (20) indicates that the uniform density and temperature case probably overestimates Λ_d since some of the dust emission will be absorbed within the cloud and will serve to heat other dust grains. Equation (20) indicates that even a B3 star will be able to maintain $T_d\sim 30$ K out to a radius of 0.5 pc.

Although the dust can be heated appreciably by an embedded source with fair ease, whether the gas will also be heated is a more involved question. Many heating and cooling processes must be considered. Goldsmith and Langer (1978) have calculated the total cooling rate via molecular and atomic lines, as a function of gas density and temperature. For a uniform density sphere with a diameter of 1 pc, we find the total cooling rate is

$$\Lambda=0.58\,L_\odot\left[\frac{T_k}{30\,\mathrm{K}}\right]^{2.7}\left[\frac{2R}{1\,\mathrm{pc}}\right]^3 \quad \text{for } n(\mathrm{H}_2)=10^4\,\mathrm{cm}^{-3} \tag{21a}$$

$$=2.93\,L_\odot\left[\frac{T_k}{30\,\mathrm{K}}\right]^{2.9}\left[\frac{2R}{1\,\mathrm{pc}}\right]^3 \quad \text{for } n(\mathrm{H}_2)=10^5\,\mathrm{cm}^{-3}. \tag{21b}$$

To balance this cooling rate, various heating mechanisms were considered by Scalo (1977) and by Goldsmith and

To balance this cooling rate, various heating mechanisms were considered by Scalo (1977) and by Goldsmith and Langer (1978). We calculate for the above model cloud

$$\Gamma_{cr} = 2.5\times10^{-2}\, L_{\odot}\left[\frac{n(H_2)}{10^4\,cm^{-3}}\right]\left[\frac{2R}{1\,pc}\right]^3, \tag{22a}$$

$$\Gamma_{comp} = 4.3\times10^{-2}\, L_{\odot}\left[\frac{n(H_2)}{10^4\,cm^{-3}}\right]^{3/2}\left[\frac{2R}{1\,pc}\right]^3\left[\frac{T_k}{30\,K}\right], \tag{22b}$$

$$\Gamma_{is} = 2.07\, L_{\odot}\left[\frac{n(H_2)}{10^4\,cm^{-3}}\right]^{7/6}\left[\frac{2R}{1\,pc}\right]^{3/2}\left[\frac{B_0}{1\mu G}\right]^3\left[\frac{T_k}{30\,K}\right]^{1/4}\left[\frac{\xi_M}{10^{-6}}\,\frac{\zeta(H_2)}{2\times10^{-17}}\right]^{-1/6}, \tag{22c}$$

where Γ_{cr}, Γ_{comp}, and Γ_{is} are the heating rates by cosmic rays, compression against purely thermal support, and the magnetic ion-neutral slip. We have assumed the magnetic field to be $B = B_0 n(H_2)^{\gamma}$, where $B_0 = 1$ microgauss is the appropriate value for the interstellar medium at $n(H_2) = 1\ cm^{-3}$. We adopt the maximum value for the index $\gamma = \frac{2}{3}$ corresponding to a frozen-in magnetic field, in order to maximize Γ_{is}.[5] We note that if $\gamma = 1/2$ as suggested by Mouschovias (1976), $\Gamma_{is} \propto [n(H_2)]^{2/3}$, so that our calculated value of Γ_{is} in equation (22c) is lower by two orders of magnitude. This can be compensated by an increase in B_0 by a factor of 5. The heating rate from the formation of H_2 was also considered by Goldsmith and Langer, and was judged to be smaller than Γ_{cr} in steady state.

From equation (22), we expect Γ_{is} to be the dominant heating mechanism as compared to Γ_{cr} and Γ_{comp}. By comparing to equation (21), we see that $\Gamma_{is} \gtrsim \Lambda$ until $R \gtrsim 1$ pc for $n(H_2) = 10^4\ cm^{-3}$, and $R \gtrsim 2.5$ pc for $n(H_2) = 10^5\ cm^{-3}$. However, for low temperatures such as $T_k \sim 10$ K, even Γ_{cr} and Γ_{comp} will be important heating rates because of the strong dependence of Λ on T_k.

The role of the UCHII regions in heating the gas can finally be evaluated by considering gas-dust collisions (Spitzer 1949). We find a heating rate

$$\Gamma_{gd} = 5.2\times10^{-3}\, L_{\odot}\left[\frac{n(H_2)}{10^4\,cm^{-3}}\right]^2\left[\frac{2R}{1\,pc}\right]^3\left[\frac{T_k}{30\,K}\right]^{1/2}[T_d - T_k], \tag{23}$$

where we have assumed the grain radius $s = 6\times10^{-6}$ cm ($\Gamma_{gd} \propto s^2$), and a sticking coefficient of 0.5 (Leung 1975). It is clear from equation (23) that dust heating of the gas will be important only for the high density and/or high dust temperature regions. Both Γ_{gd} and Λ as expressed in equations (21) and (23) have been scaled up from rates per H_2 molecule. Thus equating Γ_{gd} and Λ per molecule will constrain $T_d(r)$ as a function of T_k and $n(H_2)$ if dust heating is to be dominant. Applying this result to equation (20), we derive a relation for the effective radius R_{eff} at which an embedded source will be able to heat the gas to a temperature T_k:

$$\frac{2R_{eff}}{1\,pc} \approx \left[\frac{L^*}{10^4\,L_{\odot}}\right]^{1/2}\left[\frac{50\,K}{T_k + \Delta T(T_k/30\,K)^{\delta}}\right]^{(4+\alpha)/2}, \tag{24}$$

where $\Delta T = T_d - T_k$ is the temperature required for the dust to heat the gas at $T_k = 30$ K, ΔT scales with T_k to the power of δ, and α is the power law index of the emissivity, $0 < \alpha < 2$; both ΔT and δ are functions of $n(H_2)$: $\delta = 2.2(2.4)$, $\Delta T = 112$ (5.6) K for $n(H_2) = 10^4(10^5)\ cm^{-3}$. Equation (24) is plotted in Figure 8. Note that increasing L_* by a factor of ~ 10 (changing spectral types from B0.5 to O7) increases R_{eff} by only a factor of 3. From Figure 8 we conclude that unless $n(H_2) \gtrsim 10^5\ cm^{-3}$, dust heating of the gas via gas-grain collisions must be confined spatially on a scale $\lesssim 0.1$ pc for $T_k \gtrsim 30$ K. We emphasize that equation (24) is based on inferred dust properties. Furthermore, R_{eff} is strictly an upper limit since radiative transfer has not been properly treated (Scoville and Kwan 1976); however, this serves to strengthen the above conclusion.

These calculations serve to delineate the role of the compact H II regions in the energetics of the molecular clouds under various physical conditions as deduced from our data. We conclude that the CHII and UCHII regions represent embedded sources that will easily heat extended regions of dust. With $T_d \gtrsim T_k$, dust cooling of the gas will not occur, so

[5] We have followed Goldsmith and Langer (1978) in expressing the ion abundance as a function of the gaseous metal abundance ξ_M and the cosmic ray ionization rate ζ, based on the model of Oppenheimer and Dalgarno (1974). However, we followed Scalo (1977) in allowing for the ion slip velocity to be substantially greater than the thermal velocity which is as expected in the higher density regime. The values of Γ_{is} as calculated by Goldsmith and Langer are lower for $n(H_2) > 10^3\ cm^{-3}$.

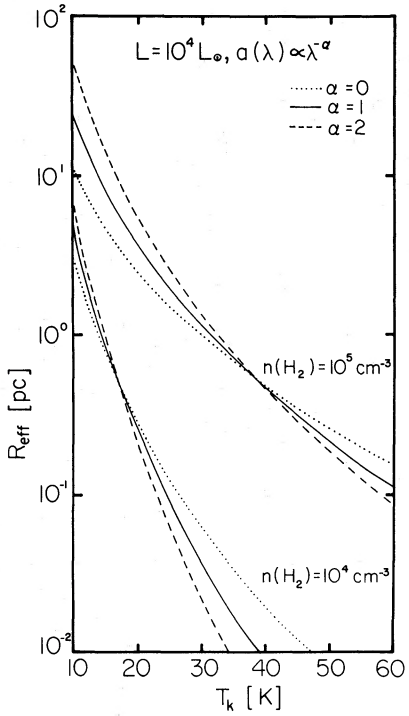

FIG. 8.—Radius $R_{\rm eff}$ at which an embedded source can still heat the gas via gas-dust collisions. The calculations are performed for a B0.5 star with $L_* = 10^4\ L_\odot$. $R_{\rm eff}$ scales as $L_*^{1/2}$. The different curves correspond to different values for the emissivity index α, and density $n(H_2)$.

the principal coolants for the gas are the allowed molecular and atomic transitions. If the dust is to collisionally heat the gas to $T_k \gtrsim 30$ K over the observed size scales, we require $n(H_2) \gtrsim 10^5$ cm^{-3}. Alternatively magnetic ion-neutral slips appear capable of heating the gas if an initial field $B_0 \sim 1$ microgauss is frozen in during the early stages of collapse. We comment that if a more efficient scheme for coupling the gas to grain works—e.g., via infrared excitation of H_2O molecules (Scoville and Kwan 1976; Takahashi, Hollenbach, and Silk 1981)—the magnetic field alternative can be avoided at a lower gas density.

Hence in the context of energy balance, and to explain the size scale of heated gas, a clumpy cloud model is consistent with dust heating via collisions. In the unclumped cloud model where $n(H_2) \gtrsim 10^4$ cm^{-3}, alternative means for heating the gas, such as the relaxation of an embedded magnetic field, will be required.

IV. CONCLUSIONS

Molecular lines of NH_3, CS, and CO are used to study the cloud environment in which CHII and UCHII regions are embedded. We find that typically small (R less than a few pc), warm ($T_k = 20$–40 K), dense [$n(H_2) > 10^4$ cm^{-3}], and massive ($M = 10^2$–$10^4\ M_\odot$) clouds are associated with each of these regions. In each case the UCHII region is found to peak with the NH_3 emission. We argue that they probably correspond to density maxima, although they are in general also associated with temperature maxima.

Despite our efforts to measure the size of the NH_3 emission regions by comparing observations made with different antenna beamwidths, and our efforts to deduce the densities by comparing NH_3 and CS observations, we cannot rule out the possibility of many small distinct clumps within the antenna beam. We suggest two possible models for these clouds: (1) The NH_3 emission regions *are not* severely clumped. Typical size scale of these regions is then 1–3 pc with substructures of the order of 1 pc. Densities are modestly high with $n(H_2) \sim 10^4$ cm^{-3}. These clouds constitute a major fraction of the total H_2 column density along the line of sight. Although the embedded H II regions will easily heat the dust, gas densities are too low for the dust to heat the gas directly via collisions. Unless energy can be transferred more efficiently from the dust to gas, we must appeal to magnetic ion-neutral slips for the primary heating source for the gas. (2) The NH_3 emission regions *are* severely clumped. Typical size scale is then ~ 0.1 pc. Observations with 43″ resolution then suggest the presence of small hot cores. Densities within the clumps are high, with $n(H_2) \gtrsim 10^5$ cm^{-3}.

Despite the possibility of many clumps within the beam, these are small condensations so that the bulk of the H_2 column density along the line of sight lies outside of the clumps. Densities are also high enough now that dust will directly heat the gas, at least within the clumps.

Masses for these regions are fairly well determined. This, together with the fact that UCHII regions are small, implies that initial masses for these regions can be reliably estimated. We find that stars earlier then B0 are not found in the less massive regions. The apparent ability of the later spectral types to accrete a large fraction of the initial cloud mass implies either that the angular momentum of the cloud has been dissipated early on, or that the cloud density was already substantial [$n(H_2) > 10^3$ cm^{-3}] before the final collapse and fragmentation as described by Larson (1978). For the early O stars, we argue that interaction of clumps as in coagulation theories may be a possible explanation for the observation that these stars are found only in the more massive regions.

We wish to thank the staff of the Haystack Observatory and the NRAO, and Bob Loren of the MWO, for their assistance during our observations. We also thank Malcolm Walmsley and Frank Israel for many helpful suggestions on the manuscript. P.T.P.H. acknowledges support from the Miller Institute for Basic Research. This research was also supported in part by NSF grants AST76-24610, AST77-12960, and AST78-21037.

REFERENCES

Barrett, A. H., Ho, P. T. P., and Myers, P. C. 1977, *Ap. J. (Letters)*, **211**, L39.
Beetz, M., Elsasser, H., Poulakos, C., and Weinberger, R. 1976, *Astr. Ap.*, **50**, 41.
Beichman, C. A., Becklin, E. E., and Wynn-Williams, C. G. 1979, *Ap. J. (Letters)*, **232**, L47.
Blair, G. N., Evans, N. J., II, Vanden Bout, P. A., and Peters, W. L., III. 1977, *Ap. J.*, **219**, 896.
Blair, G. N., Peters, W. L., and Vanden Bout, P. A. 1975, *Ap. J. (Letters)*, **200**, L161.
Bodenheimer, P. 1978, *Ap. J.*, **224**, 488.
Davidson, K., and Harwit, M. 1967, *Ap. J.*, **148**, 443.
Dickel, J. R., Dickel, H. R., and Wilson, W. J., 1978, *Ap. J.*, **223**, 840.
Dickman, R. L. 1975, *Ap. J.*, **202**, 50.
_____. 1978, *Ap. J. Suppl.*, **37**, 407.
Downes, D., Genzel, R., Moran, J. M., Johnston, K. J., Matveyenko, L. K., Kogan, L. R., Kostenko, V. I., and Ronnang, B. 1979, *Astr. Ap.*, **79**, 233.
Downes, D., and Wilson, T. L. 1974, *Ap. J. (Letters)*, **191**, L77.
Dyck, H. M., and Capps, R. W. 1978, *Ap. J. (Letters)*, **220**, L49.
Dyck, H. M., and Simon, T. 1977, *Ap. J.*, **211**, 421.
Evans, N. J., Beckwith, S., Brown, R. L., and Gilmore, W. 1979, *Ap. J.*, **227**, 450.
Evans, N. J., II, Beichman, C., Gatley, I., Harvey, P., Nadeau, D., and Sellgren, K. 1981, *Ap. J.*, in press.
Evans, N. J., II, Blair, G. N., and Beckwith, S. 1977, *Ap. J.*, **217**, 448.
Evans, N. J., II, Plambeck, R. L., and Davis, J. H. 1979, *Ap. J. (Letters)*, **227**, L25.
Fazio, G. G., Lada, C. J., Kleinmann, D. E. Wright, E. L., Ho, P. T. P., and Low, F. J. 1978, *Ap. J. (Letters)*, **221**, L77.
Forster, J. R., Welch, W. J., and Wright, M. C. H. 1978, *Ap. J.*, **221**, 137.
Genzel, R., and Downes, D. 1977, *Astr. Ap. Suppl.*, **30**, 145.
Glushkov, Yu, I., Denisyuk, E. K., and Karyagina, S. V. 1975, *Astr. Ap.*, **39**, 481.
Goldreich, P., and Kwan, J. 1974, *Ap. J.*, **189**, 441.
Goldsmith, P. F., and Langer, W. D. 1978, *Ap. J.*, **222**, 881.
Goss, W. M., Lockhart, K. A., Fomalont, E. B., and Hardebeck, E. G. 1973, *Ap. J.*, **183**, 843.
Goss, W. M., Matthews, H. E., and Winnberg, A. 1978, *Astr. Ap.*, **65**, 307.
Gottlieb, C. A., Ball, J. A., Gottlieb, E. W., and Dickinson, D. F. 1979, *Ap. J.*, **227**, 422.
Gottlieb, C. A., Gottlieb, E. W., Litvak, N. M., Ball, J. A., and Penfield, H. 1978, *Ap. J.*, **219**, 77.
Green, S. 1980, private communication.
Gull, S. F., and Martin, A. H. M. 1975, in H II *Regions and Related Topics*, ed. T. L. Wilson and D. Downes (New York: Springer-Verlag).
Habing, H. J., Goss, W. M., Matthews, H. E., and Winnberg, A. 1974, *Astr. Ap.*, **35**, 1.
Habing, H. J., and Israel, F. P. 1979, *Ann. Rev. Astr. Ap.*, **17**, 345.
Harris, S. 1975, in H II *Regions and Related Topics*, ed. T. L. Wilson, D. Downes (New York: Springer-Verlag).
Harvey, P. J., Booth, R. S., Davies, R. D., Whittet, D. C. B., and McLaughlin, W. 1974, *M.N.R.A.S.*, **169**, 545.
Harvey, P. J., Campbell, M. F., and Hoffman, W. F. 1977, *Ap. J.*, **211**, 786.
_____. 1978, *Ap. J.*, **219**, 891.
Ho, P. T. P., Barrett, A. H., Martin, R. N., and Myers, P. C. 1977, *Ap. J. (Letters)*, **215**, L29.
Ho, P. T. P., Barrett, A. H., Myers, P. C., Matsakis, D. N., Cheung, A. C., Chui, M. F., Townes, C. H., and Yngvesson, D. S. 1979, *Ap. J.*, **234**, 912.
Israel, F. P. 1976, *Astr. Ap.*, **52**, 175.
_____. 1977, *Astr. Ap.*, **59**, 27.
Israel, F. P., Habing, M. J., and de Jong, T. 1973, *Astr. Ap.*, **27**, 143.
Israel, F. P., and Felli, M. 1978, *Astr. Ap.*, **63**, 325.
Kahn, F. D. 1974, *Astr. Ap.*, **36**, 149.
Knapp, G. L., Kuiper, T. B. M., Knapp, S. L., and Brown, R. L. 1976, *Ap. J.*, **206**, 443.
Knowles, S. M., Caswell, T. L., and Goss, W. M. 1976, *M.N.R.A.S.*, **175**, 537.
Larson, R. B. 1978, *M.N.R.A.S.*, **184**, 69.
_____. 1980, preprint.
Leung, C. M. 1975, *Ap. J.*, **199**, 340.
Leung, C. M., and Liszt, H. S. 1976, *Ap. J.*, **208**, 732.
Linke, R. A., and Goldsmith, P. F. 1980, *Ap. J.*, **235**, 437.
Liszt, H. S., and Leung, C. M. 1977, *Ap. J.*, **218**, 396.
Lo, K. Y., Burke, B. F., and Haschick, A. D. 1975, *Ap. J.*, **202**, 81.
Lo, K. Y., Walker, R. C., Burke, B. F., Moran, J. M., Johnston, K. J., and Ewing, M. S. 1975, *Ap. J.*, **202**, 650.
Loren, R. 1979, private communication.
Lucas, R. 1976, *Astr. Ap.*, **46**, 473.
Martin, R. N., and Barrett, A. H. 1978, *Ap. J. Suppl.*, **36**, 1.
Mathews, W. G. 1965, *Ap. J.*, **142**, 1120.
Matthews, H. E., Goss, W. M. Winnberg, A., and Habing, H. J. 1977, *Astr. Ap.*, **61**, 261.
McCrea, W. H., 1960, *Proc. Roy. Soc. London, A*, **256**, 245.
Mezger, P. G., Schraml, J., and Terzian, Y. 1967, *Ap. J.*, **150**, 807.
Morgan, J. M., Reid, M. J., Lada, C. J., Yen, J. L., Johnston, K. J., and Spencer, J. H. 1978, *Ap. J. (Letters)*, **224**, L67.
Morris, M., and Knapp, G. R. 1976, *Ap. J.*, **204**, 415.
Morris, M., Zuckerman, B., Palmer, P., and Turner, B. E. 1973, *Ap. J.*, **186**, 501.
Mouschovias, T. Ch. 1976, *Ap. J.*, **207**, 141.
Myers, P. C., Ho. P. T. P., and Benson, P. J. 1979, *Ap. J. (Letters)*, **233**, 441.
Oka, T. 1968, *J. Chem. Phys.*, **49**, 3135.
Oppenheimer, M., and Dalgarno, A. 1974, *Ap. J.*, **192**, 29.
Panagia, N. 1973, *A. J.*, **78**, 929.
Pipher, J. L., and Soifer, B. T. 1976, *Astr. Ap.*, **46**, 153.
Plambeck, R. L., and Williams, D. R. W. 1979, *Ap. J. (Letters)*, **227**, L43.
Rieke, G. H., Low, F. J., and Kleinmann, D. E. 1973, *Ap. J.*

(*Letters*), **186**, L7.
Righini-Cohen, G., and Simon, M. 1977, *Ap. J.*, **213**, 390.
Ryle, M., and Downes, D. 1967, *Ap. J.* (*Letters*), **148**, L17.
Scalo, J. M. 1977, *Ap. J.*, **213**, 705.
Scoville, N. Z., and Kwan, J. 1976, *Ap. J.*, **206**, 718.
Scoville, N. Z., and Solomon, P. M. 1974, *Ap. J.* (*Letters*), **187**, L67.
Schwartz, P. R. 1979, *Ap. J.* (*Letters*), **229**, L45.
Schwartz, P. R., Cheung, A. C., Bologna, J. M., Chui, M. F., Wauk, J. A. and Matsakis, D. 1977, *Ap. J.*, **218**, 671.
Sibille, F., Lunel, M., and Bergeat, J. 1976, *Astr. Ap.*, **47**, 161.
Silk, J., 1978, in *Protostars and Planets*, *IAU Colloquium No.* 52, ed. T. Gehrels (Tucson: University of Arizona Press).
Silk, J., and Takahashi, J., 1979, *Ap. J.*, **229**, 242.
Spitzer, L., Jr. 1949, *Ap. J.*, **109**, 337.
Takahashi, J., Hollenbach, D., and Silk, J. 1981, in preparation.
Ulich, B. L. 1979, private communication.
Ulich, B. L. and Haas, R. W. 1976, *Ap. J. Suppl.*, **30**, 247.
Vanden Bout, P. A., Loren, R. B., Snell, R. L., and Wooten, H. A. 1981, in preparation.
Vanderwoort, P. O. 1963*a*, *Ap. J.*, **138**, 294.
_____. 1963*b*, *Ap. J.*, **139**, 869.
Wilson, T. L., Downes, D., and Bieging, J. 1979, *Astr. Ap.*, **71**, 275.
Wootten, H. A., Evans, N. J., II, Snell, R. L., and Vanden Bout, P. A. 1978, *Ap. J.* (*Letters*), **225**, L143.
Wynn-Williams, C. G., and Becklin, E. E. 1974, *Pub. A.S.P.*, **86**, 5.
Wynn-Williams, C. G., Becklin, E. E., and Neugebauer, G. 1974, *Ap. J.*, **187**, 473.
Wynn-Williams, C. G., Werner, M. W., and Wilson, W. J. 1974, *Ap. J.*, **187**, 41.

A. H. BARRETT: Department of Physics, Massachusetts Institute of Technology, Rm 26-331, Cambridge, MA 02139

P. T. P. HO: Radio Astronomy Laboratory, 601 Campbell Hall, University of California, Berkeley, CA 94720

R. N. MARTIN: Max-Planck-Institut für Radioastronomie, Auf dem Hugel 69, D-5300 Bonn 1, West Germany